



POLITECNICO DI TORINO

Master's thesis in aerospace engineering

**Analysis and calculation of a forced
response for low pressure turbine blades
with Interlocking contact**



Candidate:

Santi Carrubba

Supervisor:

Daniele Botto

Ing. Marco Moletta

October 2019

Index

1. Introduction	1
1.1 Great 2020	1
1.2 Companies and Organizations	2
1.3 Objectives of the thesis	5
2. Aeronautical Engine	7
2.1 Main existing architectures	8
2.1.1 Turbojet	8
2.1.2 Turboshaft	9
2.1.3 Turboprop	9
2.1.4 Turbofan	10
2.2 Low Pressure Turbine	14
2.3 Stator and Rotor Design	17
3. Rotordynamic	19
3.1 Static	20
3.2 Dynamic	22
3.3 Aeroelasticity	22
3.3.1 Forced Response	24
3.3.2 Flutter	29
4. Cyclic Symmetry and Modal Analysis	35
4.1 Cyclic Symmetry	35
4.2 Modal Analysis	39
4.2.1 FreND diagram	42
4.2.2 Main Modal Forms	43
4.2.3 Aliasing Phenomenon	45
5. Reduced Model analysis	47

5.1	Model Reduction	47
5.1.1	Guyan Reduction	50
5.1.2	Craig/Bampton Reduction	52
5.1.3	Tran Method	54
5.2	Linear Analysis	55
5.2.1	Blade-Disk with Shroud	56
5.2.2	FEM vs ROM	60
5.2.3	Frequency comparison	60
5.2.4	Eigenectors comparison	61
5.2.5	Contact Model	63
6.	Data Reception Procedure	65
6.1	Strain Gauges	65
6.2	Experimental Campbell	66
6.3	TEST CASE	69
7.	Conclusion	75
	Bibliography	

List of Figures

1.1 ACARE targets	1
1.2 Main aircraft engine emissions	2
2.1 Turbojet Cross Section	8
2.2 Turboshaft Cross Section	9
2.3 Turboprop Cross Section	10
2.4 Turbofan Cross Section	11
2.5 P-V and T-S diagrams of ideal Joule-Brayton cycle	13
2.6 T-S Diagram of real Joule-Brayton Cycle	13
2.7 Flow Path inside engine components	14
2.8 Low Pressure Turbine Cross Section	15
2.9 Speed triangles with $R=0$	16
2.10 Flow path inside Turbine	17
2.11 Stator Blades (a) and Rotor Blade (b)	18
3.1 Collar's Triangle	22
3.2 The forcing that excites the system at one point	25
3.3 Change of variables for a rotating system	26
3.4 Forward and Backward forcing	27
3.5 Campbell diagram with Forward and Backward frequencies	28
3.6 Campbell Diagram: for the same harmonic index, there are two rotation speed of the disk	28
3.7 Campbell Diagram	29
3.8 Two Dofs profile section	30
3.9 Damped, constant and amplified oscillations	31
3.10 Stability modes and characteristics	32
3.11 IBPA-Aerodamping Diagram	34
4.1 Cyclic symmetry example	35
4.2 Sector of a Disk	37

4.3 Representation of nodal diameter and nodal circle	39
4.4 Stationary Mode	40
4.5 Rotating Mode in Anti-Phase	41
4.6 FreND Diagram	42
4.7 Edgewise Mode	44
4.8 Flapwise Mode	44
4.9 1F Mode	44
4.10 1T Mode	44
4.11 Stripe Mode	45
4.12 Aliasing Phenomenon	46
5.1 Sector of Blade with node for reduction	54
5.2 Free Contact	57
5.3 Tight Contact	57
5.4 Full-Stick Contact	58
5.5 Frequency response with stiffness $K=K_{\text{nominal}}$	58
5.6 Frequency Response with Stiffness $K=0.1 K_{\text{nominal}}$	59
5.7 Frequency Response with Striffness $K=0.25 K_{\text{nominal}}$	59
5.8 FEM vs ROM frequency	60
5.9 FEM vs ROM Eigenvectors	61
5.10 MAC diagram	62
5.11 Contact Model	63
6.1 Strain Gauge	65
6.2 Experimental Campbell Diagram	66
6.3 Q-Factor Diagram	68
6.4 CAD of sector blade	69
6.5 Master Node on Blade	70
6.6 Mode Shape	71
6.7 Amplitude Diagram	72

6.8 Q-Factor Diagram	72
6.9 Amplitude with Experimental Data	73
6.10 Q-Factor with experimental data	74

Abstract

Nowadays the Aeronautic research field is continuously growing up due to industrialization and to the exponential global market development. The worldwide competition stimulates the research field to challenge and cross the current technology limits. The Aeronautic world is divided in two different categories: civil field and military field, for whose the research has got different targets according to the target of reference. In the military field, for example, there is a strong need to have more and more performing aircraft, also accepting lower reliability requirements, for which we tend to experiment with new concepts and new materials, and then transport this design results, adapting them according to different standards. In this sense, it aims to meet extremely stringent requirements for reliability, as well as to optimize passenger comfort and reduce the aircraft's environmental impact as much as possible. This master's thesis, developed at GE Avio Srl, is part of civil research and is part of a larger project, the GREAT 2020, which involves the development of new generation engines that move in the sense described above. The work on which the following thesis is based focuses on the vibration dynamics of turbomachinery for aeronautical application, in particular dealing with the low pressure turbine component rotors. The final aim is to validate a specific interlocking contact simulation model.

1. Introduction

1.1 Great 2020

The GREAT 2020 project was born in 2009, promoted by the Piedmont Aerospace District Committee and co-financed by the Piedmont Region with the European Regional Development Fund POR-FESR 2007-2013, with the aim of developing innovative technologies for next generation aircraft engines and to meet the demands of a constantly growing sector in order to achieve ever higher quality standards, promoting the adoption and development of sustainable solutions from an economic and ecological point of view. This has allowed technological advances that have made air transport safer, more convenient and more efficient compatibly with the challenge of "sustainable air mobility".

In detail, the aim is to halve the emissions of carbon dioxide, to reduce the emissions of nitrogen oxides by 80% and to reduce the perceived noise by 10 dB compared to the technologies used in 2000.

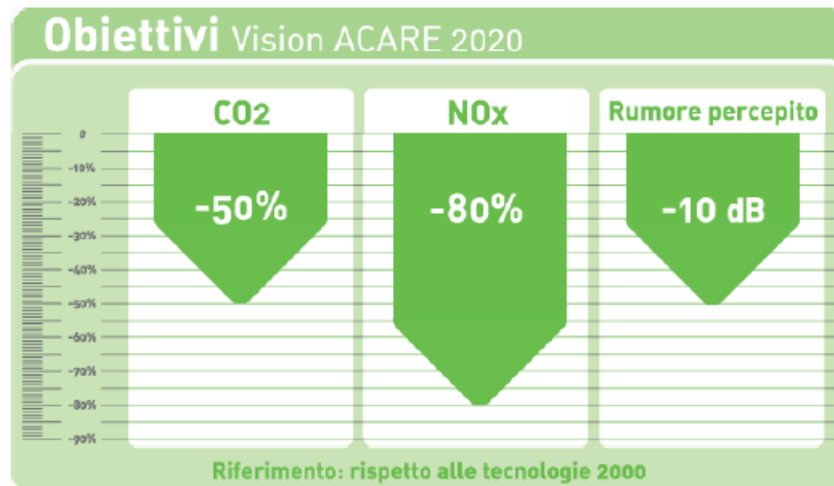


Figure 1.1: ACARE targets

In the aircraft engine the main products generated by combustion are carbon dioxide (CO₂) and nitrogen oxide (NO_x). While the amount of CO₂ is directly proportional to the amount of fuel burned, the formation of NO_x also depends on the thermal conditions of the combustion chamber: for example, at take-off, when the chamber

temperature reaches its maximum peak, NO_x emissions are maximum. The continuous increase in air traffic makes regulation and reduction of the noise emitted due to operation indispensable.

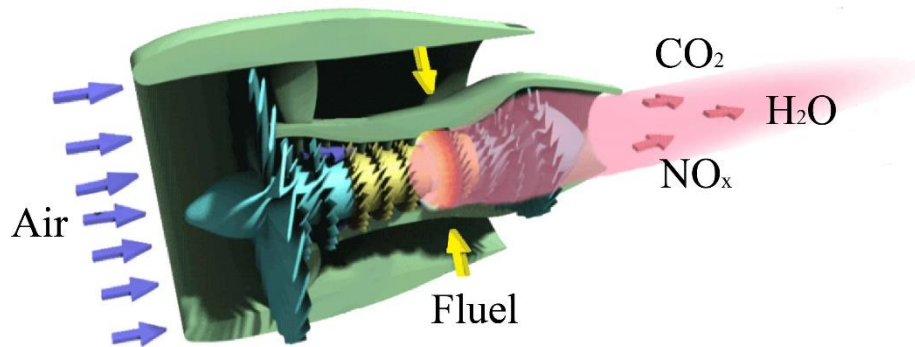


Figure 1.2: Main aircraft engine emissions

1.2 Companies and Organizations

The success of the great 2020 comes from the presence in the Piedmont area, and particular in Turin, of specialized companies, high-level university training and research centers such as "Avio Aero".

The close collaboration between companies present in the area and public bodies has enabled the development of a permanent structure for research and development of aeronautical technologies within the GREAT 2020 framework. Avio Aero, the Polytechnic of Turin and the Turin Unit of the Institute of Science and Technology of Ceramic Materials take on a leading role within the project.

- *Avio Aero*, acquired by General Electric in 2012, is a leading company in the design, production and maintenance of low-pressure turbines, gearboxes and combustors for aero-engine for civil and military aircraft, as well as in the development of new materials intended for additive manufacturing. Founded in 1908, it now has over 4800 people, of which 4200 work in Italy. The head office is located in Rivalta di Torino and houses the largest production center. Brindisi, Pomigliano d'Arco and Cameri host the other Italian establishments. As for foreign countries, the company has a production plant and a test center in Poland.

- The *Polytechnic of Turin* is known worldwide for training and research activities in the field of engineering. There are several departments involved in the GREAT2020 project, in particular: Department of Mechanical and Aerospace Engineering, Applied Science and Technology, Energy, Management and Production Engineering. The Polytechnic University of Turin actively collaborates with Avio Aero on the research topics mentioned above: from this partnership the Great Lab was born in 2008 and, more recently, the TAL (Turin Additive Laboratory).
- *ISTEC-CRN* The Institute for Science and Technology of Ceramic Materials carries out research activities aimed at the innovation of materials and processes for the satisfaction of the emerging demands of the industrial and scientific sector, both national and international. The topics of interest are many and concern in particular aerospace, biomedical, mechatronic and cultural heritage sectors. The Turin Unit of ISTEC carries out research activities within the GREAT 2020 project aimed at the development of processing and compatible systems on aeronautical use alloys.
- *Laboratories* To carry out the activity of the GREAT 2020 project, six laboratories are present in Piedmont, each of which is composed of Avio Aero engineers, researchers from the institutions mentioned above and staff from local companies. They are involved in the development of strategic technologies for the construction of new generation engines. Each laboratory focuses on a specific aspect of the aircraft engine, as described below.
- *Lift Lab*: dedicated to the development of innovative materials for low density and high strength structures, to their production and certification for use in new generation engines. It focuses on the development of high-strength steels for gears and on the construction of turbine and combustor components in titanium-aluminum alloys and cobalt chromium through additive manufacturing. Furthermore, the activities of the Lift include the study of the dynamic phenomena of the turbine, to guarantee control and maximum reliability.

- ***Aereon flux Lab***: intended for the advanced aerodynamic turbine project, optimization of cooling fluxes and reduction of noise emissions, it focuses on the phenomena of unsteady aerodynamics and on the management and efficiency of thermal phenomena.
- ***Ageades Lab***: the object of study is advanced transmission systems for innovative motor architectures, such as Geared Turbofan and Geared Open Rotor. In this laboratory we plan to design epicycloidal reduction systems, paying attention to dynamic effects; moreover, tools have been designed to predict the behavior of bearings and grooved connections in order to maximize performance and reliability.
- ***Zec Lab***: deals with the development and implementation of innovative combustion systems, with low emissions and operating with environmentally friendly alternative fuels. The performance and environmental impact of the latter are analyzed in particular, in addition to the development of configurations of Low-NOX injectors and advanced manufacturing processes for new combustors.
- ***MC Lab***: the laboratory has achieved the goal of developing intelligent diagnostic systems for mechanical transmission and integrated electric generators for more electric aircraft. The research aims at creating algorithms and advanced electronics able to monitor the status of the engine and anticipate any faults.
- ***ECOPRO Lab***: focuses on the study of innovative flexible and intelligent production systems, with limited human supervision, on the development of tools and systems for production processes with low environmental impact and on the integration of methods for the inspection of Ti-Al alloys.

1.3 Objectives of the thesis

The work of the following thesis focuses on the vibration dynamics of turbomachinery for aeronautical application, in particular dealing with the rotors of the low pressure turbine component. The final aim is to validate a specific interlocking contact simulation model by comparing the results of the analyzes carried out with experimental results, available being related to propellers in use for some time. Furthermore we want to compare this type of constraint with other models adopted so far: past works carried out by some graduate students, PhD students and engineers of Avio Aero have in fact brought to light that the simulation of the stiffness of the contact and of the friction damping of the same are better described from a particular condition in which the constraint is imposed in a specific way. This is the Full-Stick model, which suppose the contact to the shroud considering that the contact has the possibility of deforming before it can crawl. In particular, these are FEM analyzes carried out with software (in particular, the pre-processing, processing and post-processing phases were carried out with MSC Patran / Nastran and Ansys APDL) in which it is possible for the user to constrain certain nodes of the mesh to be able to classify and compare the results of the different models. The results of the analyzes carried out were compared qualitatively and quantitatively: in fact, Campbell diagrams were created for each stage, classifying the different modal families and the vibration frequencies of the most significant points so as to be able to make numerical comparisons in terms of relative errors with experimental data. The overlap of the analytical diagrams with the experimental ones has also allowed to observe also the trends of the results on the domains taken into consideration so that the prediction of the model in terms of variation of the response could also be evaluated. At the end non-linear contact analyzes are carried out which are subsequently compared with the experimental data so as to identify the appropriate damping values and contact stiffnesses.

The main phases of the work carried out were the following:

- ***Pre-processing***: creation of FEM models for different constraints.
- ***Processing***: analyzes launched for certain operating conditions.
- ***Post-processing***: modal classification and analysis of vibration frequencies with subsequent calculation of relative errors with respect to experimental results, creation of Campbell diagrams and evaluation of contact stiffness.

It is emphasized that the initial analyzes carried out have taken into account only the stiffness due to contact, while the damping due to friction between the surfaces to the shroud has been taken into consideration later: this aspect would in fact complicate the analysis, greatly increasing the computational cost. Moreover ignoring the friction damping the evaluations are more conservative since a beneficial factor for the rigidity of the system is not taken into account. Finally, it is necessary to point out that the simulations have been carried out under the hypothesis of cyclic symmetry: this allows to reduce the calculation time without affecting the precision of the analysis, despite the reality of the system does not include symmetry cyclical due to the presence of imperfections in the components, in the material or in the operation of the propeller.

2.Aeronautical Engine

In order to introduce the thesis, it is necessary to briefly present some general concepts relating to the engines used in the aeronautical field, in order to facilitate reading even by those who are not well versed in the subject. There are several architectures that are more or less suitable for meeting specific needs required by a given aircraft. In particular, in the aeronautical field there is a conceptual distinction between jet and engines: one speaks of engines in the case of organs dedicated to the generation of thrust in order to support the motion of the aircraft, while for engines are generally meant machines designed for generation of power for the various accessories and auxiliary apparatuses present on the aircraft. In the continuation of the thesis, however, the same meaning will be given to thrust generators on both nouns in order to avoid any repetitions.

A jet engine is a reaction engine discharging a fast-moving stream of fluid, or simply a jet, that generates thrust by jet propulsion. In general, jet engines are combustion engines that can be either airbreathing or non-airbreathing. Jet propulsion is a practical application of Newton's third law of motion, stating that, "for every force acting on a body there is an opposite and equal reaction". For aircraft propulsion, the "body" is atmospheric air that is forced to accelerate as it passes through the engine. The force required to give this acceleration has an equal effect in the opposite direction acting on the system producing the acceleration. A jet engine produces thrust by propelling a large weight of air backwards in the form of a very high speed jet of gas. The resultant thrust acting on the engine is given by the general thrust equation:

$$F = \dot{m}_e v_e - \dot{m}_0 v_0 + (p_e - p_0) A_e$$

where \dot{m} is the mass rate, v the air flow velocity, p the pressure and the subscripts "e" and "0" refers to the exhausted and the entering quantities respectively, and A_e is the exit area. From equation it can be noted how the same thrust can be obtained either by giving a small velocity to a large mass of air, or

vice-versa, a large velocity to a small mass of air. In practice the former is preferred, since by lowering the jet velocity relative to the atmosphere a higher propulsive efficiency is obtained.

2.1 Main Existing Architectures

2.1.1 Turbojet

It is an engine architecture developed during the Second World War by the engineers Sir Frank Whittle and Hans von Ohain. Currently this engine is in use only in the military field for high-speed performance. The initial design included a single compressor and an axial turbine mounted on the same shaft in a single compression and expansion stage. More recent concepts instead envisage having more compression and expansion stages with different parallel trees; so these processes are made gradual in order to avoid, for the compressors, phenomena of detachment of the boundary layer due to the adverse gradient and instability phenomena, while for the turbines the objective is to avoid reaching the sonic mach on the array, to avoid that the same works in a field for which it was not designed.

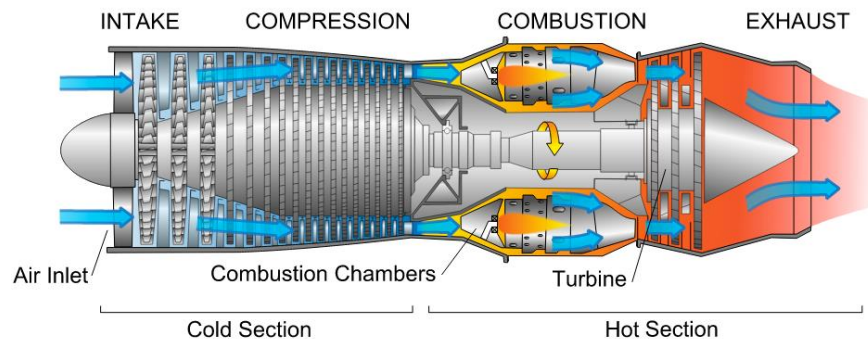


Figure 2.1: Turbojet Cross Section

Engine operation is based on an air intake that processes the air flow required by the engine, slows it down and conveys it to the compressor, that is moved by the turbine, to perform work on the fluid to pressurize it and increase its temperature adiabatically. The air intake must have a high efficiency to guarantee a certain flow rate and must correctly direct the fluid in order to avoid the distortions that would

cause the detachment of the boundary layer and three-dimensional flows. When the flow reaches the combustion chamber, heat is introduced which raises the fluid energy. The turbine expands the flow and the energy stored by the gases is converted into mechanical energy transferred to the compressor to move its components. At the same time it increases the kinetic energy of the gas through the nozzle, so as to generate the necessary thrust for the motion.

2.1.2 Turboshaft

The architecture of this engine includes a gas turbine that follows the Brayton cycle to produce power. It is mostly installed on helicopters and its configuration is very similar to the turbojet, except for the nozzle which is replaced and the helicopter's main rotor is connected.

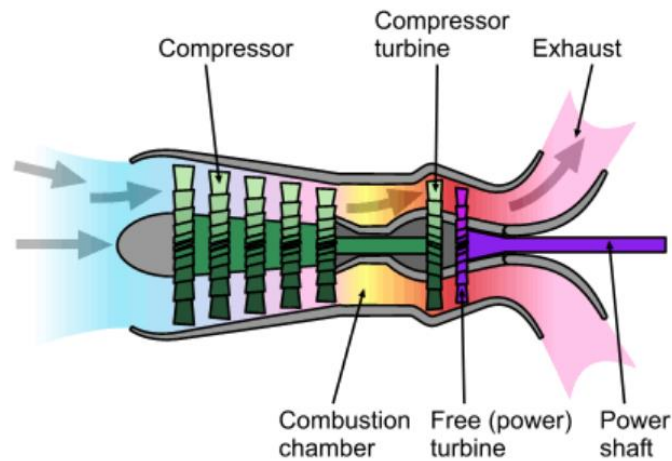


Figure 2.2: Turboshaft Cross Section

This configuration can occur both as single shaft and double shaft; in this last case, the previous complex takes the name of gas generator to which a free turbine will be connected for power generation.

2.1.3 Turboprop

The turboprop is an evolution of the turboshaft: the most commonly used scheme is the twin shaft with free power turbine. In addition to the previous one, there is also

a nozzle for thrust generation. Between the turbine shaft, which supplies power, and the propeller, there is a reducer.

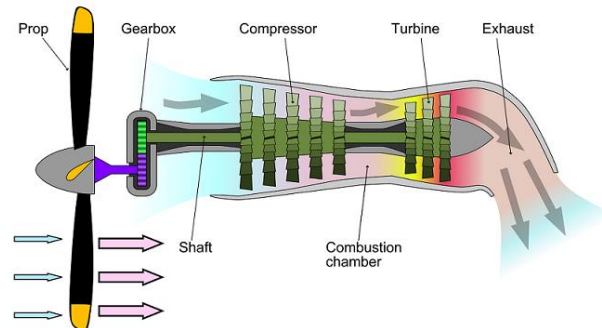


Figure 2.3: Turboprop Cross Section

The advantages of this architecture are lower consumption than any other configuration. The reduced specific consumption is the result of the high air flow rate elaborated by the propeller: this allows, with the same thrust, to have to accelerate the flow in smaller quantities. However, the propeller has operating problems for Mach greater than 0.5. A further development of this technology, known as Propfan, envisages acting on the propeller profile to reach Mach of the order of 0.7.

2.1.4 Turbofan

It is a type of engine widely used on aircraft currently in existence. It has all the basic components installed on the turbojet, with an additional turbine, located before the exhaust nozzle. The architecture a of turbofan engine is quite simple.

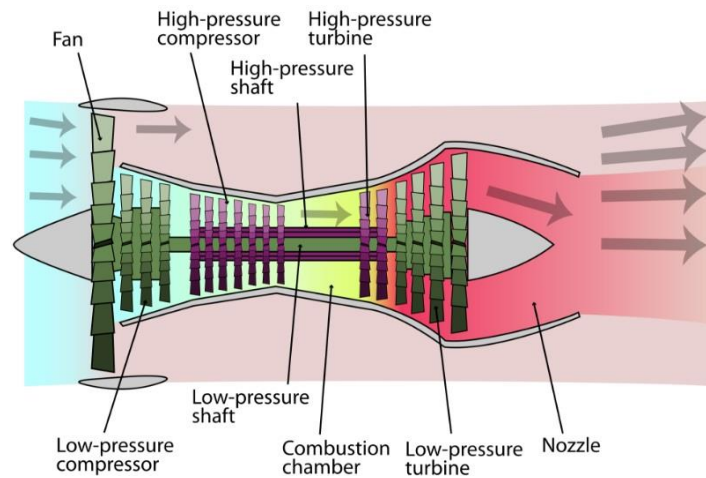


Figure 2.4: Turbofan Cross Section

For instance the cross-section of a typical dual-shaft engine is shown; The main components are:

- *Air Intake:* all turbine engine have an air intake, to bring free stream air into the engine. Generally has divergent shape in order to decelerate the air flow.
- *Fan and low pressure compressor (LPC):* consists of one or two stages, each of which is included by rotating blades mounted on a disk, followed by stators. While the LPC has the important role to perform an initial compression of the air flow, the Fan contributes to the engine's thrust by accelerating the cold air flow. The stator vanes, fixed on the engine case, are necessary to straighten the air flow to the axial direction, but they can be also useful to perform a secondary flow compression by means of an opportunely design of the air ducts between airfoils of adjacent blades.
- *High Pressure Compressor (HPC):* it is consists of several stage (10-12 or more) connected with high pressure shaft. This component increases the pressure of the fluid more, reaching even compression ratios of 30 times, consequently increasing the temperature of the fluid.
- *Combustion Chamber:* has the task of burning large quantities of fuel, supplied through several fuel spray nozzles, with extensive volumes of air in order to release the heat in such a manner that the air is expanded and

accelerated. The amount of fuel added to the air will depend upon the temperature rise required. However, the maximum temperature is limited within the range of 1100 K to 1900 K by the material from which the turbine blades and nozzles are made.

- *High Pressure Turbine (HPT)*: this turbine has the task to provide the power to drive the compressor and the accessories. Is formed by few stages, typically 2-3, each one formed by a rotor following the stator. The rotor and stator airfoils are designed to provide an expansion of the flow.
- *Low Pressure Turbine (LPT)*: this turbine has the task to provide the power for LPC and fan.
- *Exhaust System*: the system is used to expel the gas into the atmosphere and therefore generate the necessary thrust. The design of the exhaust system exerts a considerable influence on the performance of the whole engine.

Turbofan uses two separated flow. The first flow, the hot flow, passes through the entire engine and undergoes the compression, combustion and expansion cycle. The second flow, called cold flow, bypasses the core going from the fan directly to the nozzle. The ratio of the mass-flow of air bypassing the engine core compared to the mass-flow of air passing through the core is the bypass ratio:

$$BPR = \frac{\dot{m}_f}{\dot{m}_c}$$

The BPR is a descriptive parameter of this type of architecture, according to which, with the same compression ratio and maximum temperature at the turbine inlet, the specific consumption of the engine decreases but the weight and the encumbrance increase markedly with the increase of the BPR itself. The limit in this sense is placed by the ever increasing dimensions of the engine. The thermodynamic cycle upon which the gas turbine engine works is, in its simplest form, the Brayton's cycle shown in Figure

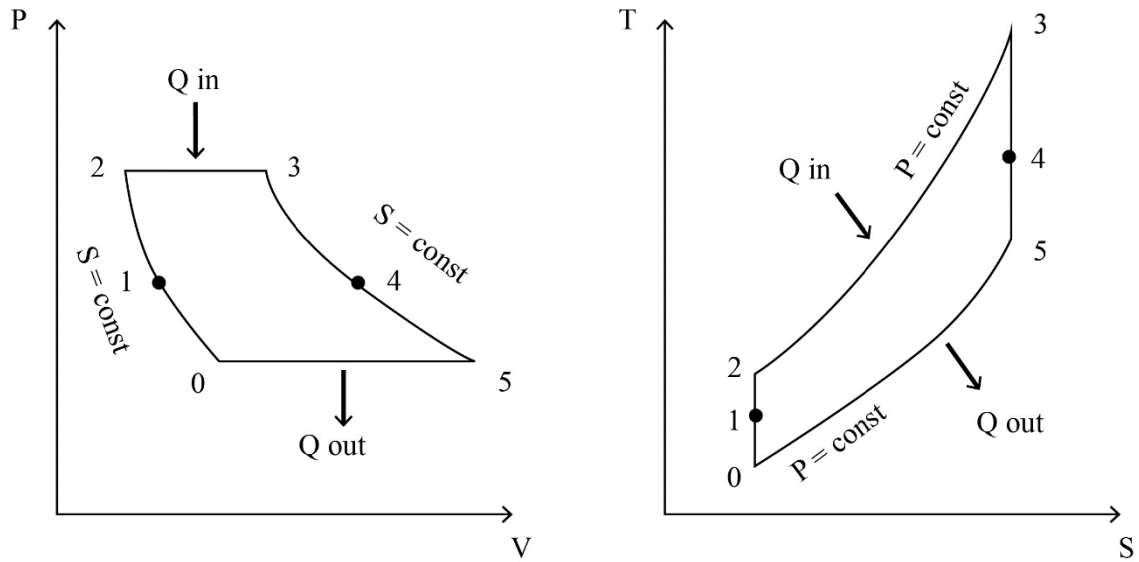


Figure 2.5: P-V and T-S diagrams of ideal Joule-Brayton cycle

The cycle starts with free stream condition at station “0”. The air intake reduces the flow speed to allow the compressor to function correctly at station “1”. As the flow slows, some of the energy associated with the aircraft velocity increases the static pressure of the air and the flow is compressed. This process is ideally isentropic and the static temperature is also increased. The compressor increases the pressure and temperature of the flow isentropically to station “2”. In reality, the compression is not isentropic and the compression process go to the right because the entropy of the flow increases.

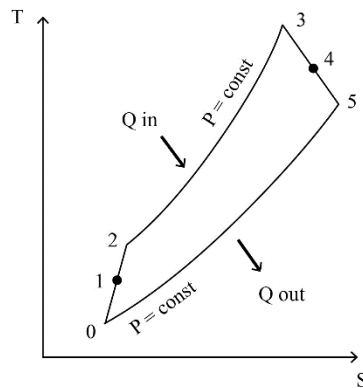


Figure 2.6: T-S Diagram of real Joule-Brayton Cycle

The combustion process in the burner occurs at constant pressure from station “2” to station “3”. The temperature increase depends on the type of fuel used and the fuel-air ratio. After that, the hot exhaust gas passes through the turbine in which the work is done by flow in station “3” and “4”. The turbine and the compressor are on the same shaft, the work done by turbine is exactly equal to the work done in the compressor. The nozzle then brings the flow isentropically back to free stream pressure from station “4” to station “5”.

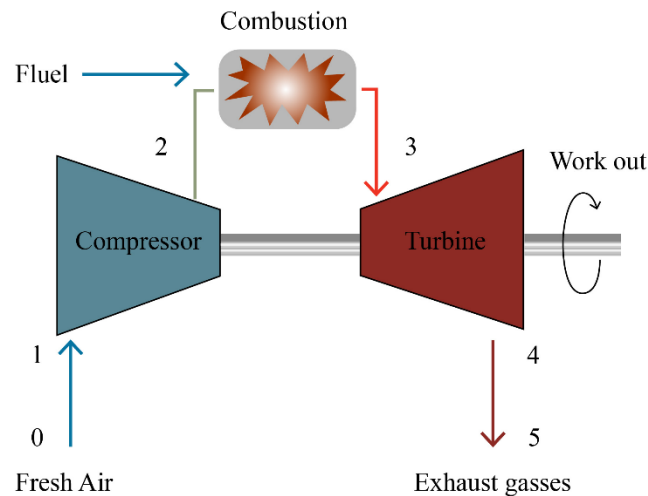


Figure 2.7: Flow Path inside engine components

2.2 Low Pressure Turbine

The turbine has the function of converting the potential energy of the fluid into the mechanical energy necessary to operate the compressor and to feed the accessory parts. Each stage is in fact composed of a stator (not rotating vanes), that directs and diverges the flow, and a rotor (rotating blades) transform the kinetic energy of the flow into mechanical work to the shaft. Due to the important pressure drop per stage, the stator and rotor blades become radially larger as we move from stage to stage to keep the axial velocity constant during gas expansion.

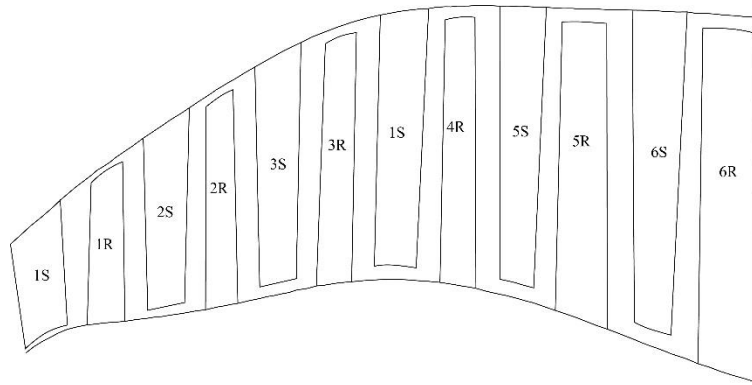


Figure 2.8: Low Pressure Turbine Cross Section

In general, the efficiencies of the turbines are higher than those of the compressors, so the expansion ratio and the work they carry out is also very high. At equal expansion / compression ratio, the turbine has a number of stages clearly lower than the compressor, as there is no positive pressure gradient (adverse gradient) which in the compressor is responsible for detachment of the boundary layer with deleterious consequences for the inter-canal. The turbine, on the other hand, has a negative pressure gradient so there is no risk of the component stalling due to the adverse gradient but due to the high speeds reached by the array it is possible to run into critical Mach phenomena, as well as the achievement of a sonic point on the profile of the blade, so that a sonic wave and a subsequent shock wave are generated. Assuming an axial turbine, from known results for turbomachinery, the work can be written for mass units:

$$\begin{cases} U_2 = U_3 = U \\ L_w = U(c_{\theta_2} - c_{\theta_3}) = c_p(T_{01} - T_{03}) \\ T_{01} = T_{02} \end{cases}$$

The design objective is to maximize the work in the turbine, an objective that can be achieved by acting on the parameters on which it depends: the peripheral speed of the blades U , the speed jump of the fluid given by the components c_{θ} , as well as the specific heat at constant pressure and the temperature jump in the turbine. This last parameter makes the turbine work proportional to the pressure drop of the turbine, through the polytropic relations. A further parameter with which the

behavior of turbomachinery can be described is called the degree of reaction; it represents the ratio between the enthalpy of the rotor and that of the stator and, for the turbine, it is thus defined:

$$R = \frac{h_2 - h_3}{h_{02} - h_{03}}$$

The design of the component is usually carried out by choosing a reaction degree $R = 0.5$ at the average radius, so that triangles of symmetrical speed and pressure jump shared equally between the stator rotor will be obtained. On the other hand, it is also possible to have $R = 0$, which represents a constant enthalpy jump across the rotor, and $R = 1$, in which the pressure jump occurs entirely in the stator. Turbines with $R = 0$ have high thrust / weight ratios but low efficiencies, so civil aircraft are usually equipped with turbines that have $R = 1$ at the medium line; they are also called “reaction turbines”.

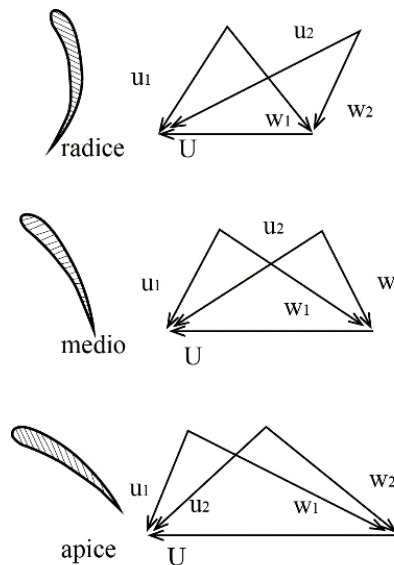


Figure 2.9: Speed triangles with $R=0$

2.3 Stator and rotor design

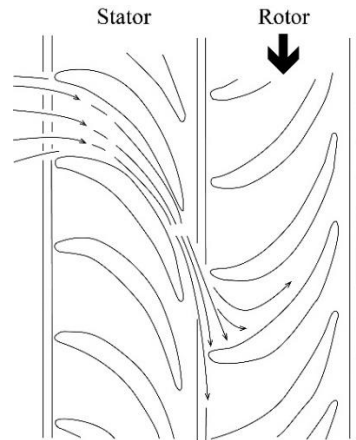


Figure 2.10: Flow path inside Turbine

As mentioned, each turbine stage is composed, in order, of a stator and a rotor. The first consists of an array of fixed blade, also called vanes, whose function is to accelerate the flow, reducing the pressure. Each blade can be considered as a beam stuck at the ends. Joints are connected to the tip and the profile hub, called respectively outer vane (OBV) and inner band (IBV). The rotor blades transfer the power from the fluid to the shaft and consist of the following elements:

1. **Airfoil**, whose shape is defined by aerodynamic requirements and obtained by interpolating the two-dimensional aerodynamic profile along the radial axis.
2. **Tip**, constitutes the roof of the blade and is located at the upper end. Contact between adjacent blade occurs at the interlock, the shroud interface surface. The creeping in this area dampens the oscillations to which the blades are subjected. The shape of the shroud is such as to guarantee an optimal contact, so that there is a high efficiency of damping .
3. **Shank**, the platform placed at the hub that supports the blade.
4. **Dovetail**, represents the connecting element between the blade and the disk slot.

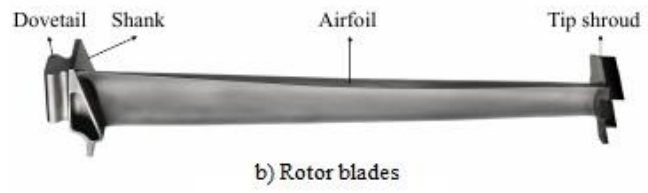


Figure 2.11: Stator Blades (a) and Rotor Blade (b)

3. Rotordynamics

As mentioned above, the stators are mainly responsible for the correct deflection of the flow to optimize the angle of attack to the rotor of the next stage optimizing the expansion. Instead rotors are instead dedicated to extracting the maximum work possible from the expanding flow, so as to be able to transmit the rotation to the shaft and consequently to the compressor and the fan. Therefore, considering the rotor, the blade interacts with the flow, while the disk has the task of transmitting the power and torque to the transmission shaft, as well as supporting the blades and resisting the centrifugal force to which they are subjected. Often the transmission of the torque is managed by a gearbox, so as to optimize the use even at rotation speeds that are very different from the design conditions.

During operation, the rotor is subject to various types of load such as the thermal, inertial and aerodynamic.

Another type of classification is possible using their trend over time:

1. *Static Load*: they are those loads that remain constant over time or that have a slow variation.
2. *Almost Static Load*: caused by dynamic phenomena, but with characteristics substantially static and therefore similar to the previous group. An example it is the centrifugal stress acting in steady state, after the end of the phenomena transient.
3. *Dynamic loads*: time-varying forces with high variation gradients, they produce non-negligible dynamic effects. Stresses of this type are for example the vibrations due to the not perfect balancing of the rotors and I aeroelastic phenomena.

3.1 Static

The task of the static analysis is to study the effects of loads on structure that they could cause excessive displacement in the structure, with consequent problems of interference, and excessive internal tension up to the break, if the limit stress is exceeded. In modal analysis for dynamics purposes, the pre-stress is only given by an inertial load and the only results considered are eigenvectors. In static analysis instead, more loads combine together, each with specific settings and specific ways.

- Inertial Load

The inertial load is the principal one acting on the structure due to the high rotational speed of aeronautical engines.

If r denotes the generic radial coordinate of a blade cross-section from the blade root and R is the maximum blade radius, the centrifugal force acting on the selected cross-section is given by:

$$F_c = \int_r^R dF_c = \rho\omega^2 \int_r^R r dV = \rho\omega^2 \int_r^R r A(r)dr$$

where ρ is the material density, ω the rotation speed and $A(r)$ the blade cross section at radius r .

- Pressure Load

Aerodynamic loads are those caused by interaction with the fluid through exchange of aerodynamic forces, they are stresses necessary to ensure the turbine to do its job. The pressure of the hot gases acting on the surface creates a bending moment which determines stresses at the root, mitigated by the inclination of the blade. The load creates a pressure distribution that varies along the radial of the blade and also along the tangential direction. In this way a flexion is generated due to the tangential force applied by the fluid and a bending due to the axial thrust determined by the pressure drop along the engine axis.

$$q_a = \rho u d (u_2 - u_1)$$

$$q_t = (P_1 - P_2) d$$

- Thermal Load

The engine components suffer a thermal deformation effect ε_T which is proportional to the difference between the temperature of the hot gases and the reference temperature at which the thermal expansion of the material is considered to be zero.

$$\varepsilon_T = \alpha(T - T_0)$$

where α is the thermal expansion coefficient. The choice of the material is very critical because with the high temperature (especially for the first rows of LPT) a sliding could also occur.

- Pre-Twist

During assembly, the low-pressure turbine blades undergo a preload of rotation around the radial axis. This procedure is necessary to optimize the position of the profile with regard to the flow during operation. Every blade is in fact pushed by adjacent blades until there is no more interference.

In the design phase it is essential to correctly assess the effects of the loads on component considering both the stresses and deformations that act, and the phenomenon of fatigue: the dimensioning must in fact take into account the resistance over the entire operating life in order to guarantee operation, with a certain margin safety, and to plan optimal maintenance intervals. Furthermore, in the aeronautical field, the performance requirement of the components is very stringent, reducing weights as much as possible and seeking solutions that respect the environment.

The design of a turbomachine must take all these factors into account, and for that reason it is translating towards increasingly less rigid and more loaded blades, also thanks to the evolution in the field of materials science and in the innovation of production technologies. However, these aspects are detrimental to the resistance of

the component to the vibrations that are created during operation, therefore a compromise must be sought between the different requirements of safety, lightness, efficiency, reliability, maintainability and reduced environmental impact.

3.2 Dynamic

The vibrations in the turbines are one of the main causes of failure and can produce resonance phenomena could lead the structure to exceed the fatigue limit and therefore cause the break. Turbine blades are particularly susceptible to high cycle fatigue damage due to the large range in frequency responses excited by the rotation, indeed, each throttle setting, means a different rotational speed, different cyclic and steady stresses induced by thermal and mechanical loads.

3.3 Aeroelasticity

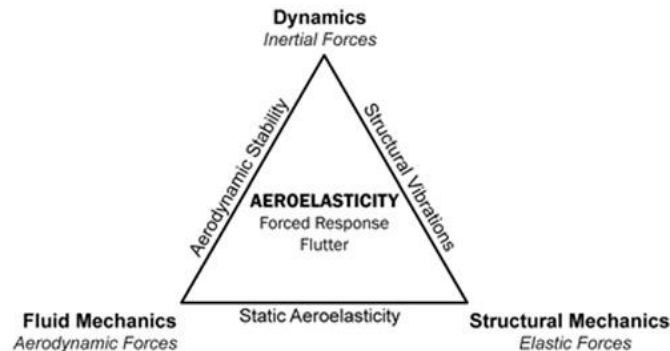


Figure 3.1: Collar's Triangle

The vibrations that occur inside the turbomachine fall within the field of aeroelasticity, which studies and describes the interaction between aerodynamic forces, elastic and inertial, both static and dynamic. In particular, how can be seen in the previous diagram, we can distinguish four fields of study:

1. Structural dynamics, if inertial and elastic forces are taken into account (this is the field that deals with structural vibrations).
2. Flight mechanics, in case inertial and aerodynamic forces are considered (aerodynamic stability).

3. Static aeroelasticity, if elastic forces and aerodynamic forces are taken into account (study of convergence).
4. Dynamic aeroelasticity, when considering the three types of forces (forced response and flutter).

The forced response analyzes a dynamic system in which the forcing is external, for example the non-uniformity of the flow that hits the turbine blade, while the flutter studies one intrinsic forcing of the system linked to the deformation that occurs under loads of various kinds and which gives rise to unsteady aerodynamic forces. The study of aerolasticity arises from the need to avoid the occurrence of torsional and flutter instability, due to the increase in operational flight speeds. They are phenomena amplified by the aerodynamic forces acting on the structure and which, with the deformation of this, they tend to diverge: in particular we speak of divergence when it comes to static rupture, while the flutter indicates a dynamic instability which tends to hunch and swing the structure to the breaking point. For each type of structure there is a natural frequency to which, by exciting the structure with a forcing, the aeroelastic phenomena are triggered. It therefore becomes fundamental study and know the resonance conditions in order to design the system or the component with sufficient safety margin. The two main types of vibrations that affect a turbine bladed disk are caused respectively by the following factors:

- the excitation of time-varying forces caused by the inhomogeneity of the flow crossing the palettes. It is linked to the architecture of the turbomachine, to the number of stator blades preceding and following the rotor and to the speed angular of the tree;
- the self-excitation that occurs in the absence of the forces when the unsteady work accomplished by the fluid prevails over the energy dissipated by the damping structure, leading to the onset of flutter.

The vibrations belonging to the first family occur at multiple frequencies of the rotation speed of the motor shaft and for this reason they are defined synchronous; this does not happen for the latter, therefore cataloged as asynchronous. Instability

a flutter constitutes a serious problem in the design phase, since, if not considered, it can cause the failure of the rotor components, particularly subject to HCF (high cycle fatigue). The study of synchronous vibrations takes place through forced response analysis, while the effect of asynchronous vibrations is evaluated with flutter analysis. Since we assume that the fluctuations caused by flutter are a lot greater than the effect of external aeromechanical forces, the latter are not considered during flutter analysis. In turn both analyzes can be linear or non-linear. The non-linearities considered in a forced response analysis of a structural and mechanical nature and reside in the presence of friction dampers. As for flutter, on the other hand, non-linearities are of interest also the flow and are represented by turbulence, shock waves and phenomena transonic.

3.3.1 Forced response

The time-varying forces that act on the turbine of an aircraft engine are caused by the disturbances generated from the upstream and downstream components of the rotor blade. They are represented as a combination of exciting harmonics traveling along the circumference of the bladed disk, which can be divided into an integer number of wavelengths, called engine order (EO), for each traveling harmonic force. Each rotor blade is therefore subject to a wide spectrum of stresses; the same applies to the statoric blades, hit by traveling forces generated by adjacent rotor trails.

Harmonic forcing is identified by the Engine order (EO), which is defined as the ratio between the pulsation of the forcing (ω) and the rotation speed of the disk (Ω):

$$EO = \frac{\omega}{\Omega}$$

In a fixed or rotating reference system with the blade there is a static forcing. Consider a bladed disk lying on the x-y plane excited at the fixed point θ^* by a harmonic forcing normal to it, directed along the z axis. The forcing is described by the following expression:

$$\begin{cases} f_{\theta=\theta^*}(t) = F_0 \cos(\omega t) = F_0 \cos(N\Omega t) \\ f_{\theta \neq \theta^*}(t) = 0 \end{cases}$$

Where ω is the pulsation of the forcing, Ω is the angular velocity of the disk and N is the number of blades.

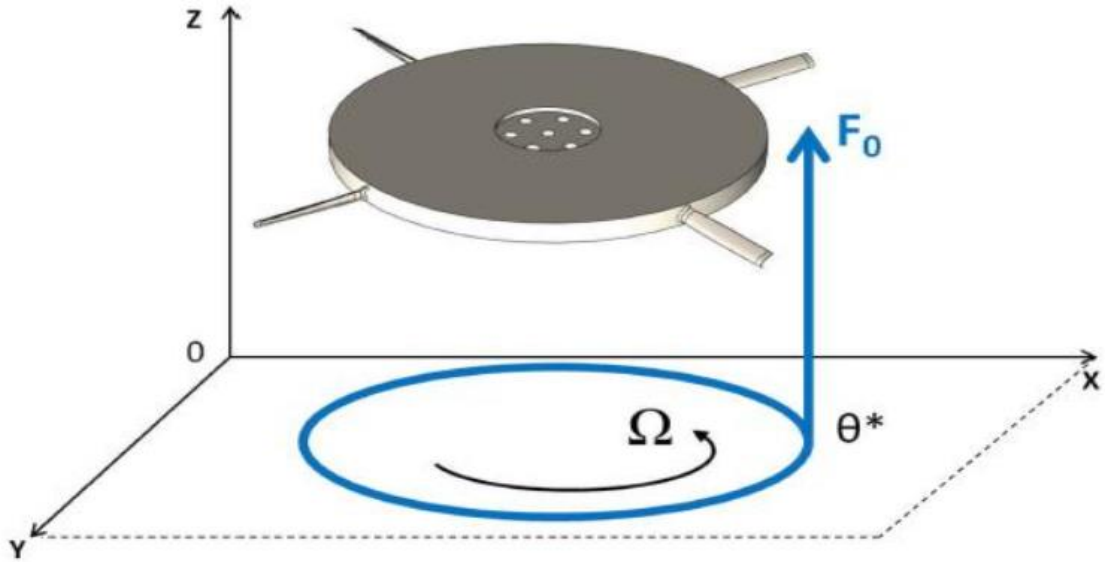


Figure 3.2: The forcing that excites the system at one point

The harmonic forcing, decomposed in Fourier series with harmonic index n :

$$f_{\theta} = \frac{F_0}{\pi} \sum_{n=0}^{\infty} \cos[h(\theta - \theta^*)] \cos(\omega t)$$

When considering a rotating reference system, a change of variable must be made.

$$\theta = \theta_r + \Omega t$$

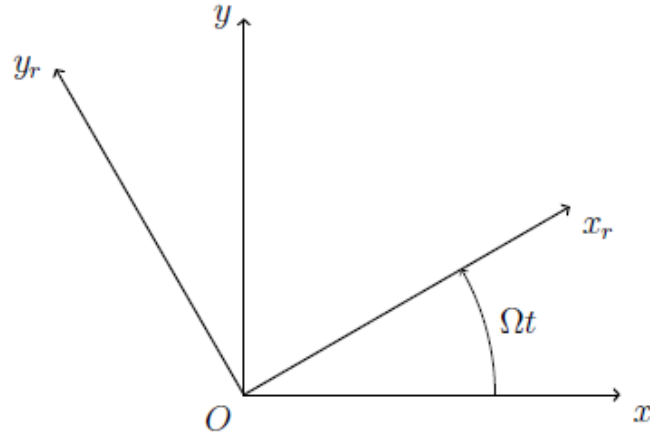


Figure 3.3: Change of variables for a rotating system

The Fourier series development is modified as follows:

$$f_{\theta,r} = \frac{F_0}{2\pi} \sum_{h=0}^{\infty} \{ \cos[(\omega - h\Omega)t] \cos(h\theta_r) + \sin[(\omega - h\Omega)t] \sin(h\theta_r) + \cos[(\omega + h\Omega)t] \cos(h\theta_r) - \sin[(\omega + h\Omega)t] \sin(h\theta_r) \}$$

The single blade is excited by two different forcing for each EO:

- *forward traveling force* concurs with the speed of rotation of the bladed disk;
- *backward traveling force* rotating in the opposite direction with respect to the speed of disc rotation.

Forcing frequencies are respectively:

$$\omega_f = \omega - h\Omega$$

$$\omega_b = \omega + h\Omega$$

The excitation frequencies are therefore a function of the forcing pulsation ω , of the number of sectors N and of the harmonic index h .

$$\Omega_f = \omega(N - h)$$

$$\Omega_b = \omega(N + h)$$

The corresponding engine orders take the following form:

$$EO_f = \frac{\Omega_f}{\omega} = N - h$$

$$EO_b = \frac{\Omega_b}{\omega} = N + h$$

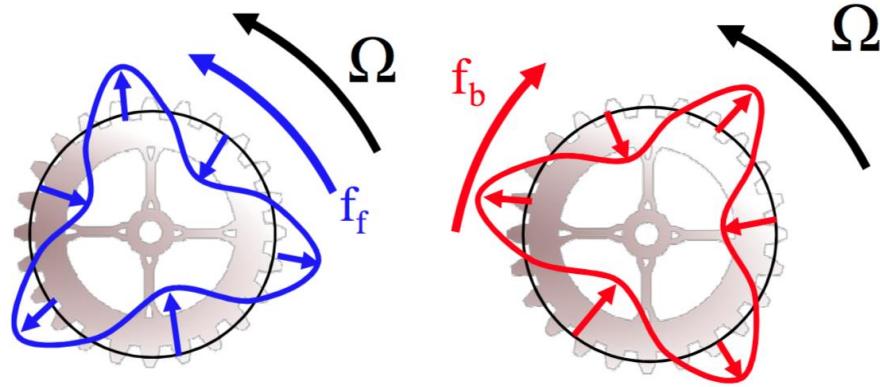


Figure 3.4: Forward and Backward forcing

$$\begin{cases} \omega_f \rightarrow f_f = \Omega \frac{EO_f}{2\pi} \\ \omega_b \rightarrow f_b = \Omega \frac{EO_b}{2\pi} \end{cases}$$

In order to study the dynamics of the rotors it is useful to observe the Campbell diagram, which shows the trend of natural frequencies as the number of turns varies: it is possible to identify potential points of resonance. This phenomenon occurs when the frequency of the periodic forcing, acting on the mechanical system, is close to the natural frequency of the system itself: vibrations of high amplitude are particularly harmful to the component. The Campbell diagram shows the rotation speed of the rotor on the x-axis and the frequency on the ordinate axis. The natural frequencies of the bladed disk are therefore represented by horizontal lines, while the frequency trend of the exciting forces is described by lines with an increasing inclination with increasing EO. Two examples of this diagram are shown below: in the first image the frequencies are highlighted forward and backward excitation in case the rotation speed is set, while in the second one shows the rotation speeds for

which is excited a generic rotary mode with f_{ris} resonance frequency since the index is imposed of Fourier harmonic.

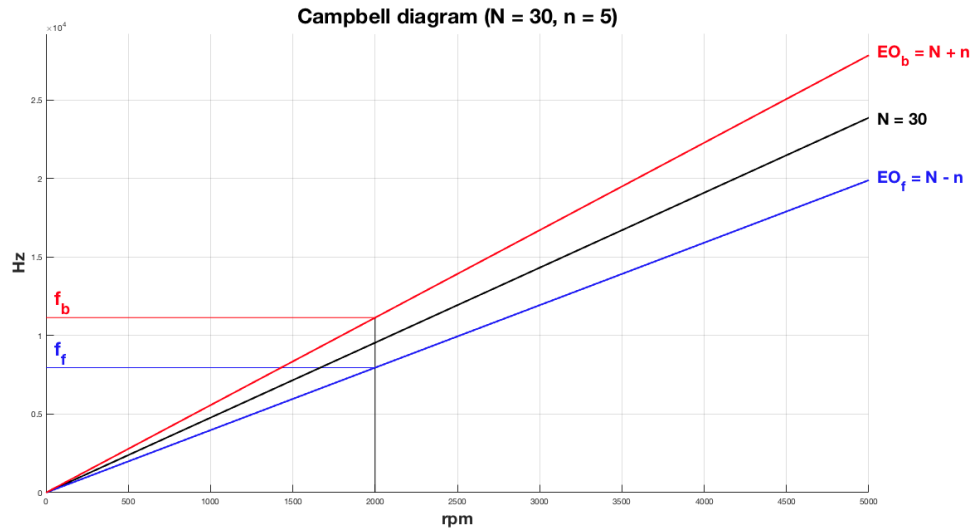


Figure 3.5: Campbell diagram with Forward and Backward frequencies

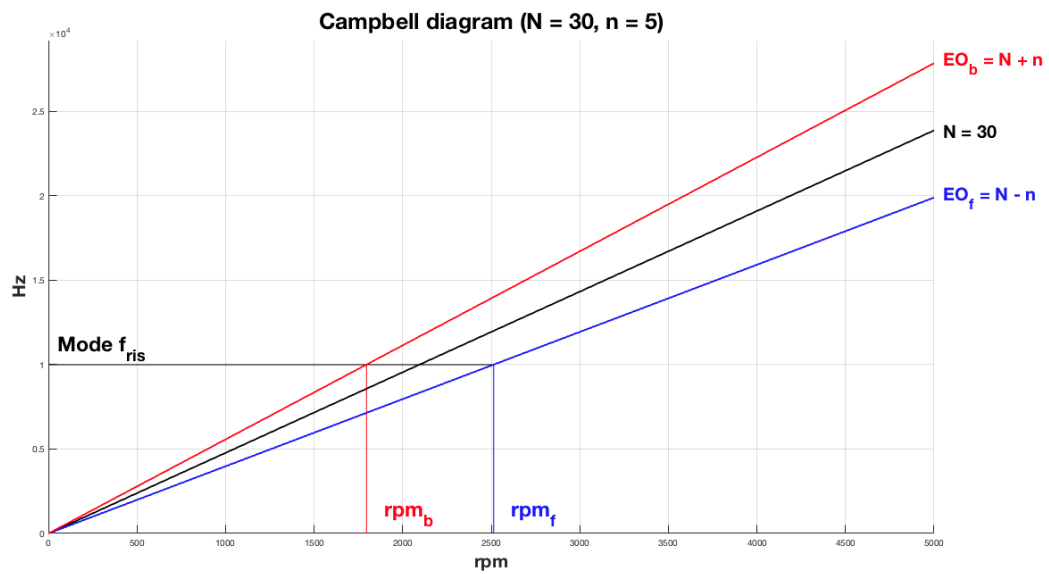


Figure 3.6: Campbell Diagram: for the same harmonic index, there are two rotation speed of the disk

This last diagram is more representative: in fact it shows crossings, intersections between a specific modal form and forcing represented by Eos. Finally a more complete diagram is shown in the following figure:

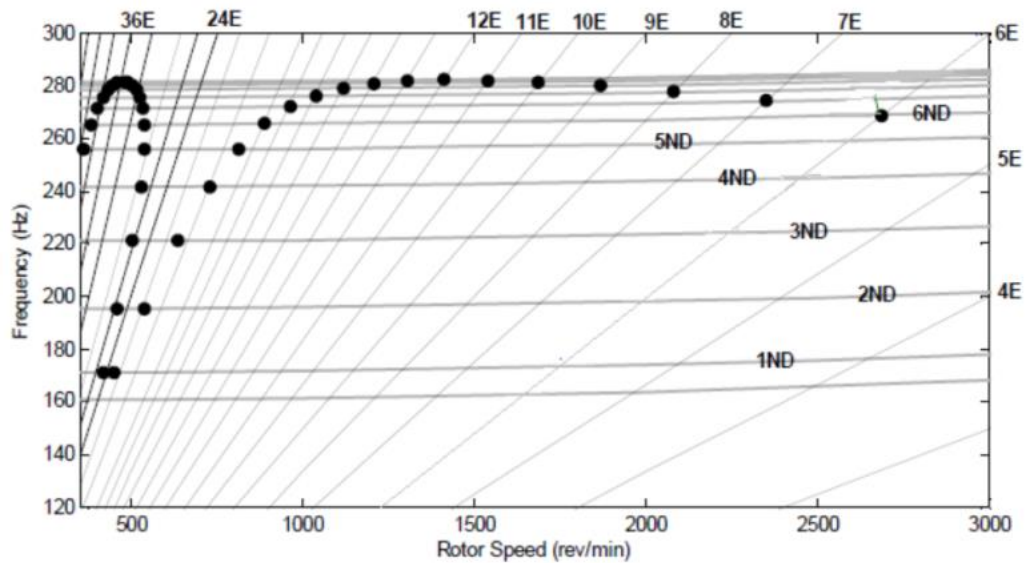


Figure 3.7: Campbell Diagram

The points at the intersection between the trend of natural frequencies and the straight lines that represent the exciters, indicate the conditions of resonance.

3.3.2 Flutter

Flutter is a self-excited and self-sustaining oscillatory phenomenon that occurs in the case in which the interaction between flow and structure brings the system to a condition of instability due to phenomena such as the separation of the current from the surface or the detachment of wake vortices downstream of the body. If the system does not come properly damped, the oscillatory amplitude increases until reaching the break.

In the aeronautical field there are two types of flutter: classic flutter and flutter in turbomachines. It can be summarized that the first deals with the structures invested by a current flow which causes instability, while in the case of turbomachinery flutter, the reciprocal influence between bodies must be considered adjacent.

Classic Flutter

Consider a simplified aeronautical structure as shown in the following figure, representing a wing profile with two DOFs (degrees of freedom). Note that the weight force W is applied in the center of gravity to the profile, which is hit by a current flow at speed U with rigid incidence α .

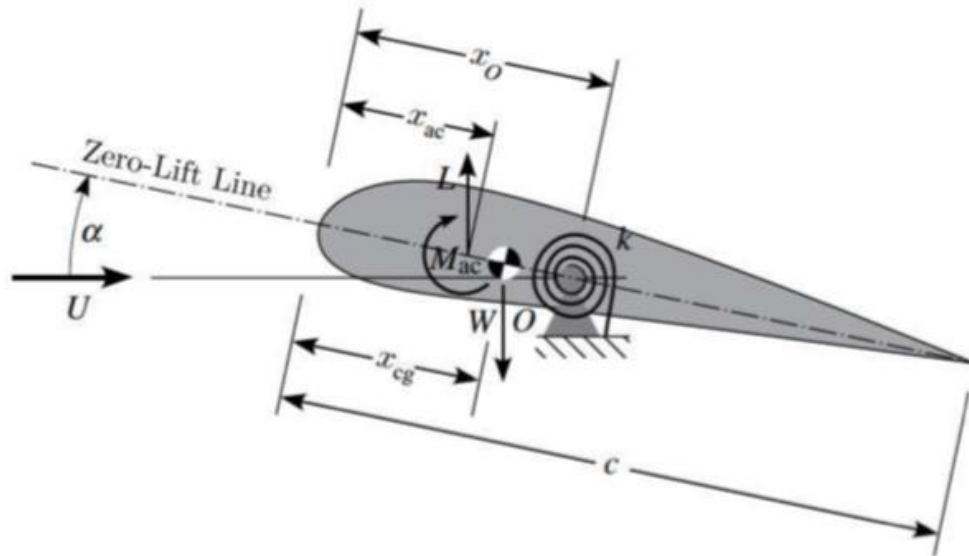


Figure 3.8: Two Dofs profile section

Aeroelasticity associates the phenomena due to forces aerodynamic, elastic and inertial.

- **Aerodynamic function** (linked to the stiffness of the profile and its shape): given an incidence α , the profile generates lift L and aerodynamic moment M_{ac} at the elastic axis of the system.
- **Elastic function** (linked to the deformability of the structure): subject to a moment, the profile rotates of an angle around its elastic axis that modify hence its aerodynamic characteristics as it changes the incidence of the flow.
- **Inertial function** (linked to the characteristic mass of the structure): date acceleration, there are inertial forces and moments acting on structure.

The aerodynamic forces also depend on the relative speed of the body immersed in the fluid.

- If $U < U_{crit}$ the oscillations are aerodynamically damped.
- If $U = U_{crit}$ the oscillations are aerodynamically supported (stability limit condition).
- If $U > U_{crit}$ the oscillations are aerodynamically amplified.

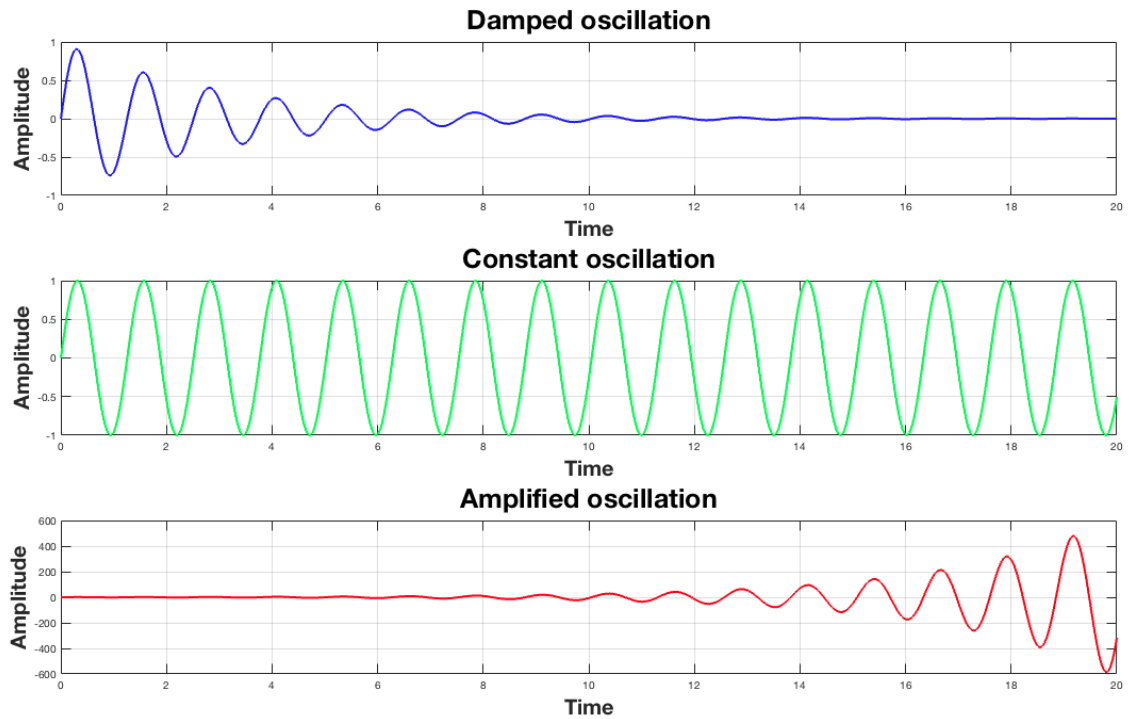


Figure 3.9: Damped, constant and amplified oscillations

Also flutter, developing into a narrow time interval, represents an extremely dangerous phenomenon in how much can determine the breaking of the structure in immediate way. This happens because the kinetic energy of the flow that feeds the vibration is much greater of the energy that the structure can absorb before catastrophic phenomena.

The mathematical system that describes the flutter phenomenon can be written in following way:

$$([K] - [K_a])\{q\} + ([D] - [D_a])\{\dot{q}\} + ([M] - [M_a])\{\ddot{q}\} = \{\lambda(t)\}$$

Where $[K]$ and $[K_a]$ are the stiffness and aerodynamic rigidity matrices, $[D]$ and $[D_a]$ are damping and aerodynamic damping matrices, $[M]$ and $[M_a]$ are mass and aerodynamic mass matrices.

This differential system is homogeneous, for which the general solution can be expressed as follows:

$$q(t) = \bar{q}_i e^{\nu t}$$

$$\lambda(t) = \bar{\lambda}_i e^{\nu t}$$

Usually the terms in λ are negligible, so in the discussion we assume that are void. The solution in this case is represented by a complex conjugate pair:

$$\nu_k = \Gamma_k \pm i\Omega_k$$

$i = 1, 2, \dots, n_c$ where n_c is the number of solutions with complex conjugate pairs. The subscript k indicates the oscillatory mode to be analyzed, while Γ and Ω are the modal damping and the modal frequency.

in short it can be stated that:

- $\Gamma < 0$ damped mode
- $\Gamma = 0$ constant mode
- $\Gamma > 0$ amplified mode
- $\Omega = 0$ static mode
- $\Omega \neq 0$ dynamic mode

Γ_k	Ω_k	MODO	STABILITÀ
< 0	$= 0$	Convergenza continua	Stabile
$= 0$	$= 0$	Tempo invariante	Stabilità limite
> 0	$= 0$	Divergenza continua	Instabile
< 0	$\neq 0$	Convergenza oscillatoria	Stabile smorzato
$= 0$	$\neq 0$	Armonica semplice	Stabilità limite
> 0	$\neq 0$	Divergenza oscillatoria	Instabile amplificato (flutter)

Figure 3.10: Stability modes and characteristics

Flutter in turbomachinery

We talk about flutter in turbomachinery when considering the mutual influence between adjacent blades: the disturbance on an element, in fact, is transmitted along the array and generates variations in the same flow that hits the blade. The movement of the blade generates aerodynamic loads non-stationary on adjacent blades that overlaps, in the hypothesis of small perturbations, to the forces caused by the interaction with the flow.

Compared to the classic flutter, it is necessary to consider the greater stiffness than characterizes the blade array. Among the parameters that most influence the vibration of a bladed – disk may include:

- Shroud, which dampens vibration due to contact friction (also it influences the modal forms and the loads at the interface.
- Shock waves, which influence the pressure loads on the blades.
- Boundary conditions (pressure, temperature, density), which influence aerodynamic damping.
- IBPA (inter blade phase angle), which affects the influence between adjacent blades, defined as

$$IBPA = \frac{2\pi n}{N}$$

where N is number of blades and n is an integer between 0 and N-1

The high ratio between the mass of the blade array and the mass of air that invests it causes the flutter in turbomachines to be a phenomenon which involves a single way of vibrating: the aerodynamic forces, lower compared to inertial forces, they are not able to cause a coupling of the ways. The flutter of a wing is instead the result of the coupling between the bending and torsional modes. The following figure shows the aerodynamic damping in function of IBPA.

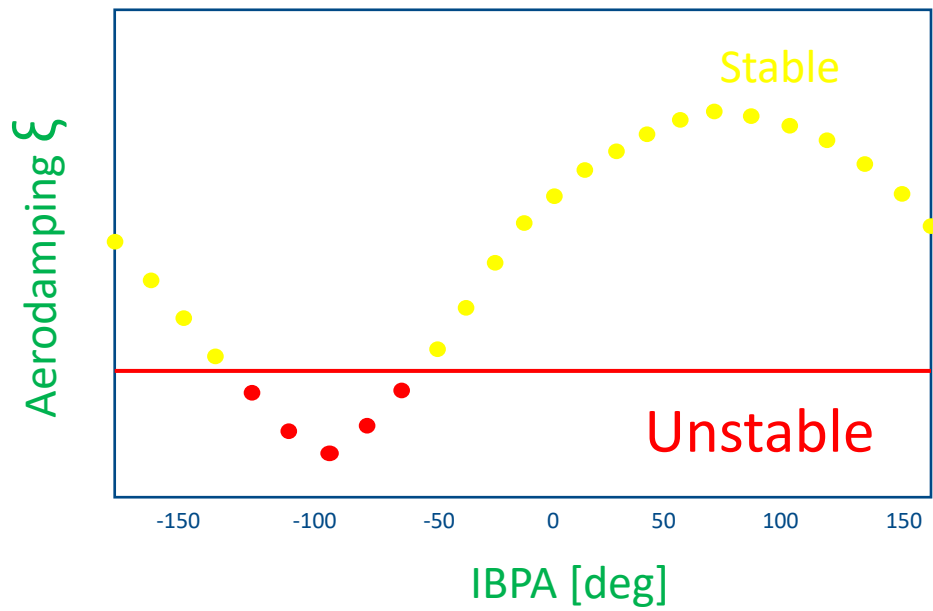


Figure 3.11: IBPA-Aerodamping Diagram

As far as turbomachinery is concerned, flutter analysis consists substantially in the calculation of an aerodynamic damping coefficient: in case it is negative instability occurs and it is necessary to operate on the parameters listed above.

4.Cyclic Symmetry and Modal analysis

4.1 Cyclic Symmetry

By definition, a structure is said in cyclic symmetry when it has a rotational periodicity and therefore is consisting of a finite number of identical sectors that form a geometry closed. The fixed and rotating parts of a turbine fall into the category of structures in cyclic symmetry. In static and dynamic simulations on very complex finite elements models, this property is useful as it allows lowering considerably the degrees of freedom of the system, with a considerable gain in terms of computational cost. But the hypothesis of cyclic symmetry does not reflect actual reality since it does not take into consideration the imperfections in the various components, both of material and in overall functioning.



Figure 4.1: Cyclic symmetry example

it is possible to subdivide the entire geometry in various sectors, defining the sector angle as:

$$\alpha_n = \frac{2\pi}{N}$$

Where N is number of blades.

The equations of motion of a system are equivalent to the number of degrees of freedom that it is characterize: a MDOF (Multi degree of freedom) system consisting of several elements is represented by the following equilibrium equation of structural dynamics:

$$[M]\{\ddot{x}\} + [C]\{\dot{x}\} + [K]\{x\} = \{F\}$$

where:

- [M] is the mass matrix and is independent of time.
- [C] is the damping matrix and is independent of time.
- [K] is the stiffness matrix and is independent of time.
- {x} is the vector of degrees of freedom and depends on time.
- { \dot{x} } and { \ddot{x} } are the first and second order time derivatives.
- {F} is the vector of external force and depends on time.

If we consider “free vibration analysis”, the vector of external force {F} is equal to zero.

The structural damping matrix is also considered equal to zero. The solution to this homogeneous problem can be written in the following way:

$$([K] - \omega^2[M])\{x\} = \{0\}$$

where ω represents the natural frequency of the system. The number of natural frequencies depends on the degree of freedom of the system. The calculation times mentioned above depend precisely on the need to solve a number of equations that is directly related to precision of the built model. Reducing the number of discretization elements thanks to the hypothesis of cyclic symmetry, it is possible to obtain a number of degrees of freedom contained and therefore it is possible to carry

out modal analyzes in a simpler way. In order to report the correct behavior of the whole structure, it is necessary to impose boundary conditions in such a way as to assert the adopted hypothesis. These hypotheses are shown in the following figure

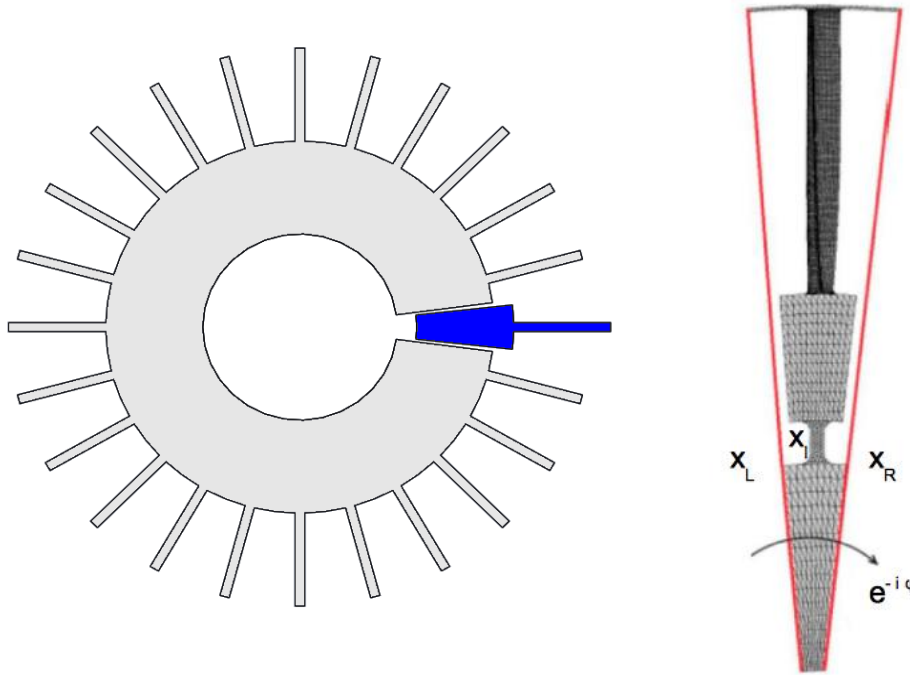


Figure 4.2: Sector of a Disk

- $\{x_l\}$ is the DOF on the Left Side
- $\{x_r\}$ is the DOF on the Right Side
- $\{x_i\}$ is a point inside the structure
- $\varphi = \frac{2\pi}{N}ND = IBPA$ is the phase
- $\{x_r\} = \{x_l\}e^{-i\varphi}$

the vector of the degrees of freedom of the single sector $\{x_s\}$ can be written in the following form, indicating with $[T]$ as transformation matrix and with CS the quantities in the condition of cyclic symmetry.

$$\{x_s\} = \begin{bmatrix} \{x_l\} \\ \{x_i\} \\ \{x_r\} \end{bmatrix} = \begin{bmatrix} 1 & 0 \\ 0 & 1 \\ e^{-i\varphi} & 0 \end{bmatrix} \begin{bmatrix} \{x_l\} \\ \{x_i\} \end{bmatrix} = [T]\{x_{CS}\}$$

$$\{F_s\} = \begin{bmatrix} \{F_l\} \\ \{F_i\} \\ \{F_r\} \end{bmatrix} = \begin{bmatrix} 1 & 0 \\ 0 & 1 \\ e^{-i\varphi} & 0 \end{bmatrix} \begin{bmatrix} \{F_l\} \\ \{F_i\} \end{bmatrix} = [T]\{F_{CS}\}$$

therefore in cyclic symmetry the equation of motion becomes:

$$([K_{CS}] - \omega^2[M_{CS}])\{x_{CS}\} = \{F_{CS}\}$$

it is possible to indicate the stiffness and mass matrices in cyclic symmetry as follows:

$$\begin{cases} [K_{CS}] = [T]^T[K_S][T] \\ [M_{CS}] = [T]^T[M_S][T] \end{cases}$$

since the force vector is null then the system equation becomes

$$([K_S] - \omega^2[M_S])\{x_s\} = \{0\}$$

the sector stiffness matrix (analogous to the mass matrix) can be expressed as a composition of the contributions of the interfaces and the interior of the sector:

$$[K_S] = \begin{bmatrix} K_{ll} & K_{li} & K_{lr} \\ k_{il} & k_{ii} & K_{ir} \\ K_{rl} & k_{ri} & k_{rr} \end{bmatrix}$$

During the vibration in a certain modal form, the sectors have a phase shift identified by the size, which can be imposed on the sector only if the interfaces are identical: in the FEM analysis phase, in fact, symmetry cyclical has validity only in the condition in which the meshes of the two surfaces they are absolutely equivalent. The relation that links the right and left interfaces of the sector is given by the following equation in which the parameter is explicit ND contained in the phase φ .

$$\{x_r\} = \{x_l\}e^{-i2\pi\frac{ND}{N}} = \{x_l\} \left[\cos\left(\frac{2\pi ND}{N}\right) - i \sin\left(\frac{2\pi ND}{N}\right) \right]$$

For the values of $\varphi = [0, \pi]$ or $ND = \left[0, \frac{N}{2}\right]$ the solution of the motion equation is real. For the remaining values instead solutions exist complex: the values are equal and opposite (opposite directions of rotation). The problem however, the eigenvalues reduce to the solution of the following equation:

$$([K_S(\varphi)] - \omega^2[M_S(\varphi)]) \begin{bmatrix} \{x_l\} \\ \{x_i\} \end{bmatrix} = 0$$

The phase angle can also equal multiples of the geometric angle, being the nodal diameter. If we indicate this multiplication coefficient with m , we must distinguish between even and odd number of sectors.

$$\begin{cases} N \text{ even:} & 0 \leq m \leq \frac{N}{2} - 1 \\ N \text{ odd:} & 0 \leq m \leq \frac{N-1}{2} \end{cases}$$

The disadvantages consist in the dependence on the nodal diameter and the need for build correct FEM models (meshes identical to the left and right interfaces of the sector).

4.2 Modal analysis

Going to analyze a body endowed with cyclic symmetry, we note that this is characterized by particular modal forms, which are characterized by two fundamental parameters:

1. nodal diameters, which represent the number of rectilinear segments defined by points with zero displacement in the deformation.
2. nodal circles, identified by the concentric circumferences constituted by the points with zero displacement in the deformation.

Modal forms can be considered as compositions of harmonic functions $\cos (ND \theta)$ and $\sin (ND \theta)$, being θ the angle at the center of the circle, that are distributed on any circumference inscribed in the bladed - disk and describe the displacements of the points belonging to it.

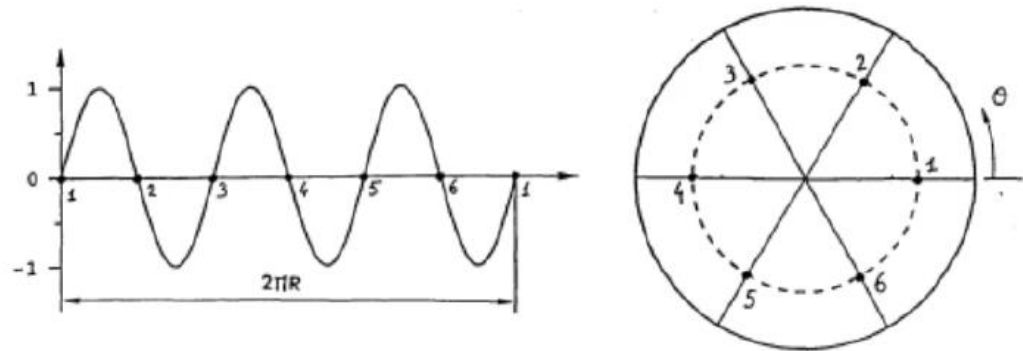


Figure 4.3: Representation of nodal diameter and nodal circle

Nodal diameters are defined as

$$\begin{cases} 0 \leq ND \leq \frac{N}{2} & \text{if } N \text{ is even} \\ 0 \leq ND \leq \frac{N-1}{2} & \text{if } N \text{ is odd} \end{cases}$$

Depending on the nodal diameter, we can divide the vibration modes into two main areas:

1. Stationary modes: all sectors vibrate with equal amplitude and phase. This condition occurs when the nodal diameter is zero or is equal to $N / 2$, therefore they are described by a single real eigenvector.

In this case, took two corresponding points on different sectors, these in every moment will have identical movements: $u(n)_i = u(n + 1)_i$

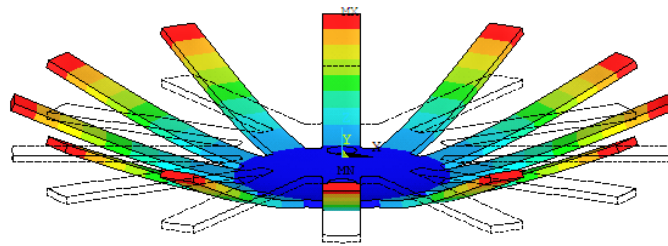
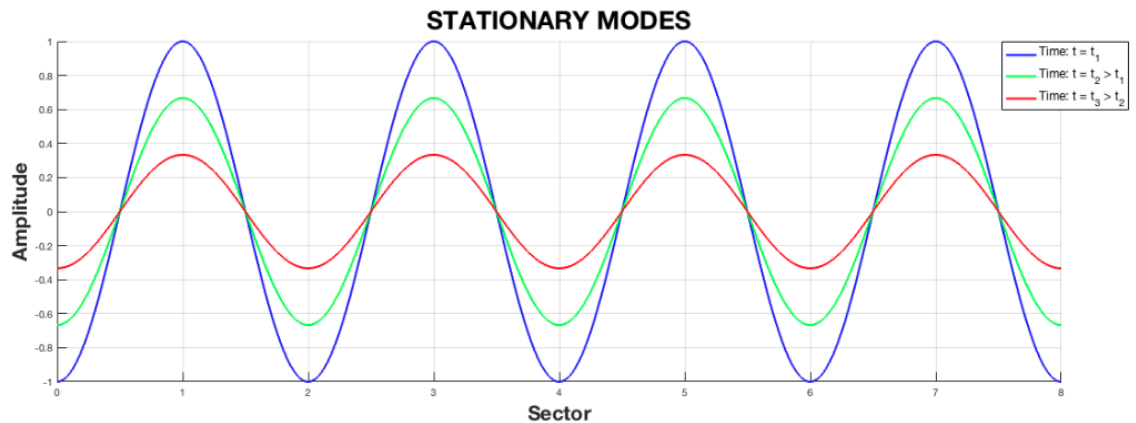


Figure 4.4: Stationary Mode



2. Rotating Modes: the modes of vibrating are characterized by a pair of waves traveling in a concordant direction and discordant with respect to the rotation of the disc. The rotating modes are described from a pair of real eigenvalues

orthogonal to each other: if the phase between the eigenvectors for the first mode is φ , the phase for the second mode is $-\varphi$ and the two rotating modes have opposite rotations. The mode of each sector is identical, but out of phase.

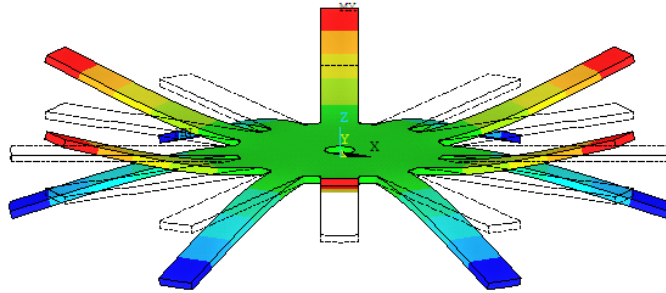
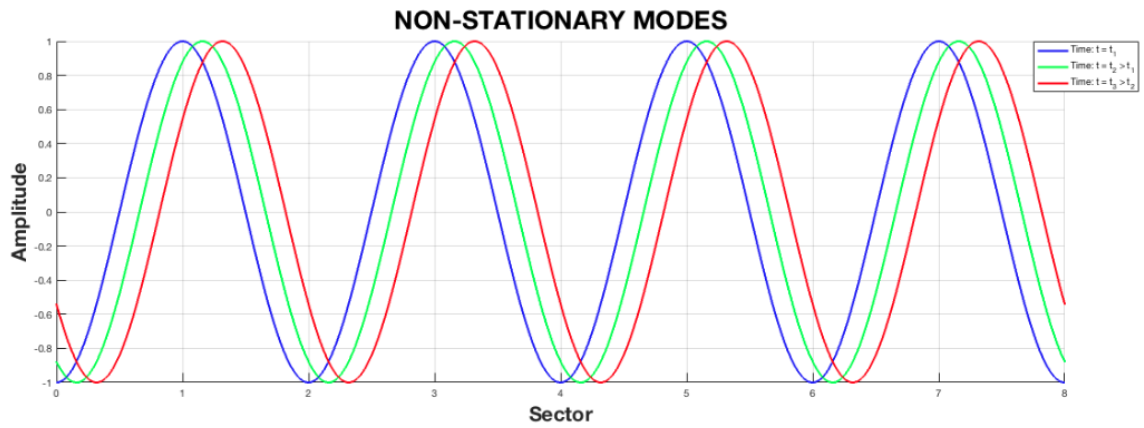
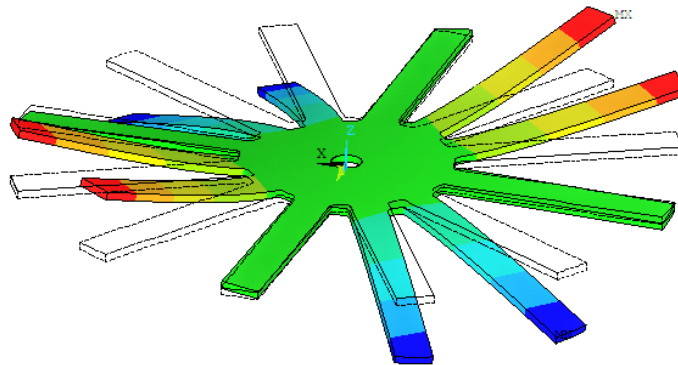


Figure 4.5: Rotating Mode in Anti-Phase



4.2.1 FreND Diagram

A real system has infinite degrees of freedom and therefore infinite ways of vibrating. Since a modeling of the system is done, we obtain a finite number of degrees of freedom and, consequently, a finite number of modes of vibration, deriving from the number of nodes used for discretization. To correctly describe the dynamics of a Blade-disk, the modes with lower resonance frequencies must be considered. The representation of the dynamic behavior is obtained thanks to the use of the FreND diagram (Frequency/Nodal Diameter).

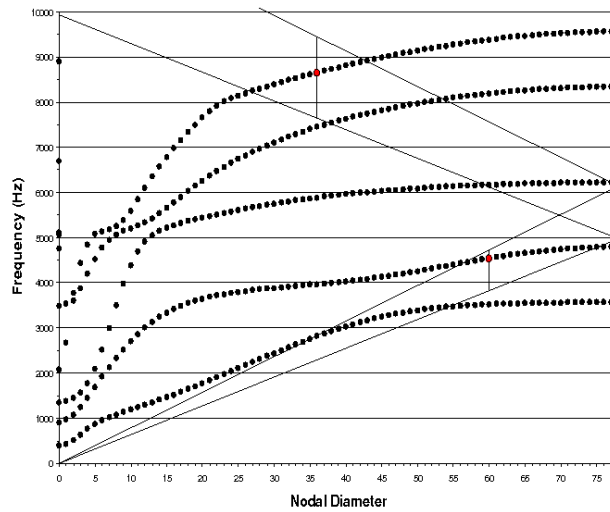


Figure 4.6: FreND Diagram

At low nodal diameters, resonance occurs at lower frequencies. As the nodal diameters grow, the frequencies increase more and more until reaching a horizontal asymptote. This happens because by increasing the nodal diameter, the points in which the displacement is zero increase and therefore the structure is globally more rigid.

We can also note that as the nodal diameters grow, the frequency growth is slower. This happens because for low nodal diameters, the disc has an important role, since the vibrations of the disc at low nodal diameters are much more marked and influence the movement of the blade. As the nodal diameters increase there is a stiffening of the disk and therefore the ways of vibrating the system become

negligible and the profile ones become more and more important. A particular area of the diagram is that in which two modal families approach each other, called Veering region. In this region the trend of the frequencies undergoes a sudden variation and the vibrations are very amplified. This is a point of particular attention especially for fatigue analysis.

4.2.2 Main modal forms

For the analyzed structures, the main modal forms can be enclosed in 6 groups:

- Edgewise (EW)
- Flapwise (FW)
- Bending (1F)
- Torsional (1T)
- Stripe (1-2S)
- Disk form

There are several other modal forms, which change with respect to the first simply by the number of half-waves. In some cases, the configuration that the deformed one assumes is an overlap of several forms, such as, for example, bending and torsion. However, these forms are not of great interest as it is known that the condition of rupture and instability occurs for minimum energy values. The less complex deformed configurations have minimal energy values.

The main deformations are shown below

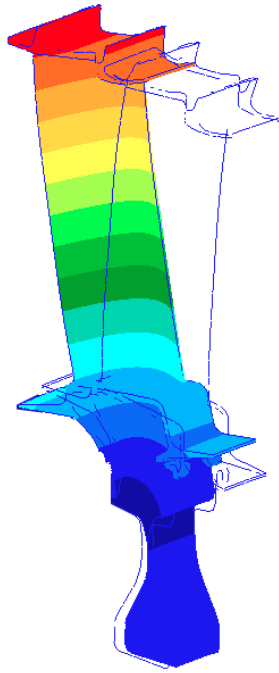


Figure 4.7: Edgewise Mode

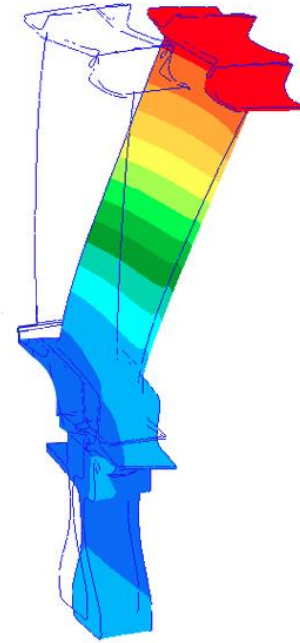


Figure 4.8: Flapwise Mode

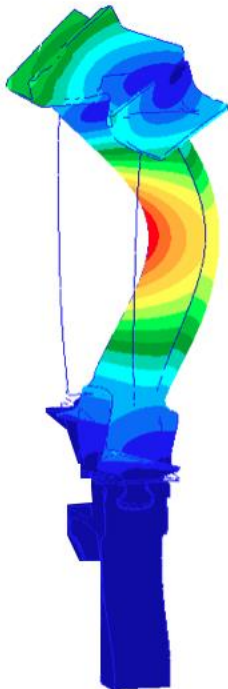


Figure 4.9: 1F Mode

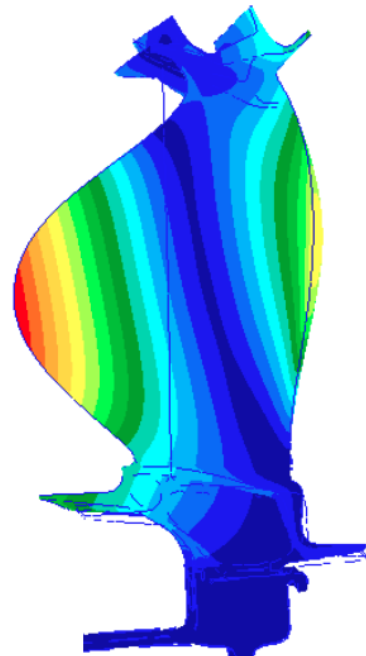


Figure 4.10: 1T Mode

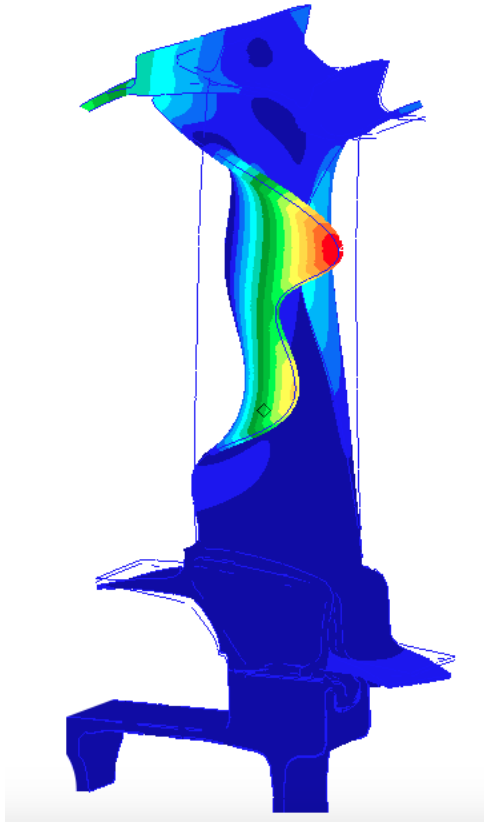


Figure 4.11: Stripe Mode

4.2.3 Aliasing Phenomenon

Taking again the Campbell diagram, the oblique lines passing through the origin, represent the EO. Resuming the previous equation is obtained

$$\omega = EO \Omega$$

Therefore the EO indicates a certain spatial periodicity of the forcing. In the case of a rotor, EO is usually dictated by the number of blades of the stator that precedes it. Being $EO = z N \pm ND$, where $z = [0,1,2,3, \dots]$, if $z = 0$ the Engine Order is equal to number of Nodal Diameter. When $z \neq 1$ an Engine Order is obtained which is not equal to the number of nodal diameters. Under this condition, the structure behaves differently by introducing the concept of aliasing.

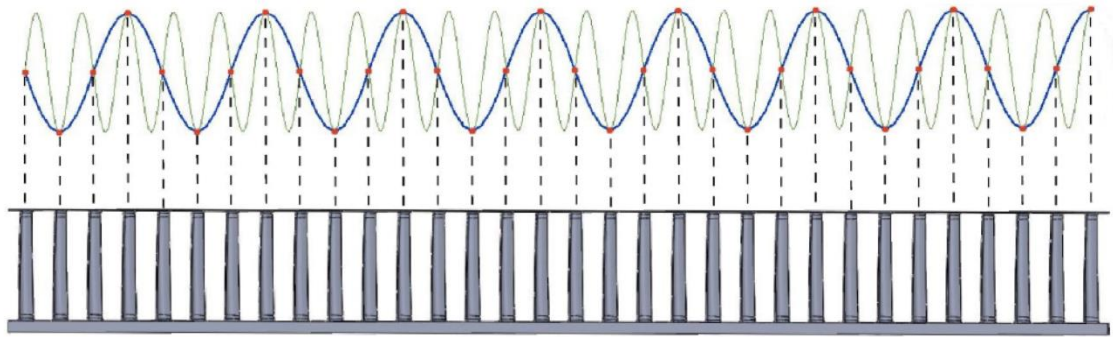


Figure 4.12: Aliasing Phenomenon

Aliasing is a phenomenon that affects the turbines, due to a discontinuity in the flow of blades in a sector. The proposed example consists of 32 sectors, so the maximum number of nodal diameters is 16. The green curve represents a force with $EO = 24$, presenting in fact 24 peaks in which the pressure is zero. Since the rotor consists of 32 blades, only a few peaks of the forcing will hit the blades, 8. Thus, a forcing with $EO = 24$ excites a modal form to $ND = 8$.

5.Reduced Model Analysis

5.1 Model Reduction

To perform the calculation of the dynamic response of a structure, use the starting FEM model, which is a model with a large number of finite elements. Using this model it is possible to derive both the mass matrix and the stiffness matrix, however it is unthinkable to perform complete dynamic analyzes, since, even considering the simplification introduced with the cyclic symmetry, the computational cost and the times are too expensive since the model remains however very complex. Depending on the displacements, the contact forces constitutes an unknown factor in the problem, therefore we must use iterative numerical methods to define the solution. The modern reduction techniques are based on the concept of “dynamic substructuring”: the structure is divided into substructures, which the dynamic response is easier to evaluate. Then the dynamic models are assembled to obtain the complete dynamic model. This procedure has advantages:

- it is possible to analyze complex structures as they are divided into subsystems.
- It allows to optimize the design based on the influence that the various components have on the overall system response;
- Replacing or eliminating components does not require the need to re-analyze the entire system. It is a fundamental aspect as it allows changes to be made by combining components belonging to different groups.

However the division of the model alone is not a sufficient simplification. It is necessary to further decrease the degrees of freedom. What you can do is use fewer nodes to define the model and then use a less dense mesh. However the reduction techniques should not cause the loss of critical information for the description of the dynamic behavior of the system. In fact a less dense mesh is unable to describe the structure, since the geometry is different from the original one and introducing a less

dense discretization, it leads to higher stress peaks that do not occur in the real case. For this reason a method is introduced which is called "model order reduction" which replaces the degrees of physical freedom with a lower number of modal degrees of freedom.

For each component of the structure “c”, we start with the usual linear equation that describes the forced response of the system:

$$M^c \cdot \ddot{x}^c(t) + K^c \cdot x^c(t) = f^c(t)$$

Where M and K are respectively mass and stiffness matrix, with dimensions NxN, $x(t)$ is the vector of degrees of freedom, with dimension Nx1, and $f(t)$ is the vector of forces, with dimension Nx1. Three categories of degrees of freedom are distinguished:

1. Accessory or active degrees of freedom (x_a), formed by all degrees of freedom on which forcing is applied or whose response is to be known.
2. Interface degrees of freedom (x_i), formed by the DOFs that belong to several adjacent components.
3. Internal or excess degrees of freedom (x_e), formed by degrees of freedom that do not belong to the previous groups.

Indicating x_b the vector $\{x_a^T, x_i^T\}^T$, the equation can be rewritten as:

$$\begin{bmatrix} M_{bb} & M_{be} \\ M_{eb} & M_{ee} \end{bmatrix} \cdot \begin{Bmatrix} \ddot{x}_b \\ \ddot{x}_e \end{Bmatrix} + \begin{bmatrix} K_{bb} & K_{be} \\ K_{eb} & K_{ee} \end{bmatrix} \cdot \begin{Bmatrix} x_b \\ x_e \end{Bmatrix} = \begin{Bmatrix} f_b \\ f_e \end{Bmatrix}$$

Vibration and static mode can be divided into two parts

$$x_e = x_e^s + x_e^d$$

the first part is a static term and can be rewritten as a function of x_b by imposing the zero accelerations and remembering that on the internal nodes dynamic forcing is not applied $f_e = 0$.

$$\begin{bmatrix} K_{bb} & K_{be} \\ K_{eb} & K_{ee} \end{bmatrix} \cdot \begin{Bmatrix} x_b \\ x_e^s \end{Bmatrix} = \begin{Bmatrix} f_b \\ 0 \end{Bmatrix}$$

$$K_{eb} \cdot x_b + K_{ee} \cdot x_e^s = 0$$

$$x_e^s = -K_{ee}^{-1} \cdot K_{eb} \cdot x_b = \Psi_{eb} \cdot x_b$$

The second part is a dynamic term that is formed by the sum of a vibration modes “ nv ”

$$x_e^d \approx \sum_{j=1}^{nv} \phi_{e,j} \eta_j = \Phi_v \eta_v$$

where the vibration modes $\phi_{e,j}$ are obtained solving the eigenvalue problem for the DoFs in x_e :

$$(K_{ee} - \omega_{e,j}^2 M_{ee}) \phi_{e,j} = 0$$

replacing in the equations is obtained

$$x_e \approx \Psi_{eb} \cdot x_b + \Phi_v \eta_v$$

By modifying the starting equation it is possible to write:

$$x = \begin{Bmatrix} x_b \\ x_e \end{Bmatrix} \approx \begin{bmatrix} I_{bb} & 0_{bv} \\ \Psi_{eb} & \Phi_v \end{bmatrix} \begin{Bmatrix} x_b \\ \eta_v \end{Bmatrix} = Rq$$

Where R is the transformation matrix and q is the reduced vector of DoFs, which is often referred to as generalized coordinates vector. by introducing the residual “ r ”, which is the difference between the exact and the approximated equation:

$$MR\ddot{q} + KRq = f + r$$

$$R^T MR\ddot{q} + R^T KRq = R^T f + R^T r$$

by imposing the Galerkin method $R^T r = 0$ it is possible to obtain an equation similar to the starting one.

$$\tilde{M}\ddot{q} + \tilde{K}q = \tilde{f}$$

Where $\tilde{M} = R^T M R$, $\tilde{K} = R^T K R$ and $\tilde{f} = R^T f$.

The Policontact software uses two CMS reduction techniques, which are then combined as required by the Tran technique. Below is a brief description of the implemented methods, referring to the case of a bladed-disk. It is important to remember that the reduced component is always more rigid than the starting model, as fewer nodes are involved. However, by analyzing the reduced model you will get slightly higher frequencies than the starting model.

5.2 Guyan Reduction

The Guyan reduction is a static reduction since it does not take into account the effect of the modal degrees of freedom.

is indicated with $\{x\}$ the vector of the degrees of freedom of the model considered, highlighting the free $\{x_f\}$ and restricted $\{x_r\}$ degrees of freedom.

$$\{x\} = \begin{Bmatrix} x_f \\ x_r \end{Bmatrix}$$

the equation of motion is the following

$$[M]\{\ddot{x}\} + [C]\{\dot{x}\} + [K]\{x\} = \{F\}$$

considering only the free degrees of freedom it's possible to rewrite the equation as:

$$[M_f]\{\ddot{x}_f\} + [C_f]\{\dot{x}_f\} + [K_f]\{x_f\} = \{F_f\}$$

in the case of a static analysis, the derivatives with respect to time are canceled.

$$[K_f]\{x_f\} = \{F_{f_static}\} = \{P_f\}$$

The free degrees of freedom can be divided into "Master" DOFs and "Slave" DOFs

$$\{x_f\} = \begin{Bmatrix} x_m \\ x_s \end{Bmatrix}$$

And the equation can be written as $\begin{bmatrix} K_{mm} & K_{ms} \\ K_{sm} & K_{ss} \end{bmatrix} \begin{Bmatrix} x_m \\ x_s \end{Bmatrix} = \begin{Bmatrix} P_m \\ P_s \end{Bmatrix}$

$$[K_{sm}]\{x_m\} + [K_{ss}]\{x_s\} = \{P_s\}$$

It's possible to obtain the vector of "Slave" DOFs:

$$\{x_s\} = -[K_{ss}]^{-1}[K_{sm}]\{x_m\} + [K_{ss}]^{-1}\{P_s\}$$

introducing the Guyan matrix defined as

$$[G_{sm}] = -[K_{ss}]^{-1}[K_{sm}]$$

$$\{x_s^s\} = [K_{ss}]^{-1}\{P_s\}$$

We can obtain $\{x_s\} = [G_{sm}]\{x_m\} + \{x_s^s\}$

The motion of the system turns is only function of master degrees of freedom. if a static analysis is performed, then the vector $\{P_s\}$ is a known term that contains the static loads, so the motion equation is completely independent of the slave DOFs. If a dynamic analysis is performed instead in $\{P_s\}$ there are also known terms representative of dynamic loads, in addition to non-linear terms related to slave DOFs. For this reason it is not possible to eliminate the dependence on the latter. The slave DOFs are therefore obliged to move according to the deformation imposed by the master displacements, considering the vector $\{P_s\}$ null and neglecting $\{x_s^s\}$. This approximation leads to writing

$$\{x_s\} = [G_{sm}]\{x_m\}$$

The columns of the Guyan matrix represent the deformations of the structure in static conditions and the elements of each column are the displacements of the Slave DOFs for the deformed one. Returning to the starting equation we can write:

$$\{x_f\} = \begin{Bmatrix} x_m \\ x_s \end{Bmatrix} = \begin{bmatrix} I \\ G_{sm} \end{bmatrix} \{x_m\} = [\Psi_G]\{x_m\}$$

We can obtain

$$[\Psi_G]^T ([M_f][\Psi_G]\{\ddot{x}_f\} + [C_f][\Psi_G]\{\dot{x}_f\} + [K_f][\Psi_G]\{x_f\}) = [\Psi_G]^T \{F_f\}$$

That becomes

$$[M_G]\{\ddot{x}_f\} + [C_G]\{\dot{x}_f\} + [K_G]\{x_f\} = \{F_G\}$$

To reduce a system by ensuring a good approximation of the behavior overall dynamic, it is appropriate:

- include nodes with the largest mass in $\{x_m\}$
- include in $\{x_s\}$ the nodes that make a negligible contribution to energy kinetics and damping
- distribute master's degrees of freedom evenly on the model
- apply loads only to master nodes.

5.3 Craig-Bampton Reduction

cyclic symmetry is an example of sub-structuring, in fact the behavior of the entire system is simulated by studying a single component. The CMS (Component Mode Synthesis) requires that the degrees of freedom of each substructure be divided into internal DOFs and boundary DOFs. The internal DOFs are those that belong to the single sector and can be considered as "slaves", while the boundaries are those that are shared between the adjacent sectors and can be considered as "masters". Unlike the Guyan reduction, in this case some modal forms are considered and, consequently, the "slave" degrees of freedom can be written as:

$$\{x_s\} = [G_{sm}]\{x_m\} + [\Phi_s]\{\eta_s\}$$

to calculate the previously omitted modal forms, the nodes at the interface are considered blocked $\{x_m\} = \{0\}$

$$[M_{ss}]\{\ddot{x}_s\} + [K_{ss}]\{\dot{x}_s\} = \{0\}$$

The solution is

$$\{x_s\} = [\Phi_s^{tot}]\{\eta_s^{tot}\}$$

Where $[\Phi_s^{tot}]$ is the modal transformation matrix, whose columns are constituted by the vibrating modes of the structure. The vector $\{\eta_s^{tot}\}$ is the vector of modal

coordinates. If we consider all the vibration modes, then the number of degrees of freedom would remain unchanged since we would have only applied a change of coordinates from $\{x_s\}$ to $\{\eta_s^{tot}\}$. If, on the other hand, we consider no vibration modes, then we would fall back into Guyan's static sub-structure. Therefore, as the modes of vibration that appear in the reduction increase, the value of the approximation increases.

$$\begin{Bmatrix} x_f \\ x_s \end{Bmatrix} = \begin{Bmatrix} x_m \\ \eta_s \end{Bmatrix} = \begin{bmatrix} I & 0 \\ G_{sm} & \Phi_s \end{bmatrix} \begin{Bmatrix} x_m \\ \eta_s \end{Bmatrix} = [\Psi] \begin{Bmatrix} x_m \\ \eta_s \end{Bmatrix}$$

In this way the "master" degrees of freedom include both the physical interface degrees of freedom and the "slave" degrees expressed as a function of the modal coordinates.

the equation of motion becomes

$$[\Psi]^T \left([M_f][\Psi] \begin{Bmatrix} \ddot{x}_m \\ \ddot{\eta}_s \end{Bmatrix} + [C_f][\Psi] \begin{Bmatrix} \dot{x}_m \\ \dot{\eta}_s \end{Bmatrix} + [K_f] \begin{Bmatrix} x_m \\ \eta_s \end{Bmatrix} \right) = [\Psi]^T \{F_f\}$$

If we impose

$$[M_{cms}] = [\Psi]^T [M_f] [\Psi]$$

$$[C_{cms}] = [\Psi]^T [C_f] [\Psi]$$

$$[K_{cms}] = [\Psi]^T [K_f] [\Psi]$$

$$\{F_{cms}\} = [\Psi]^T \{F_f\}$$

We can rewrite:

$$[M_{cms}] \begin{Bmatrix} \ddot{x}_m \\ \ddot{\eta}_s \end{Bmatrix} + [C_{cms}] \begin{Bmatrix} \dot{x}_m \\ \dot{\eta}_s \end{Bmatrix} + [K_{cms}] \begin{Bmatrix} x_m \\ \eta_s \end{Bmatrix} = \{F_{cms}\}$$

5.4 Tran Method

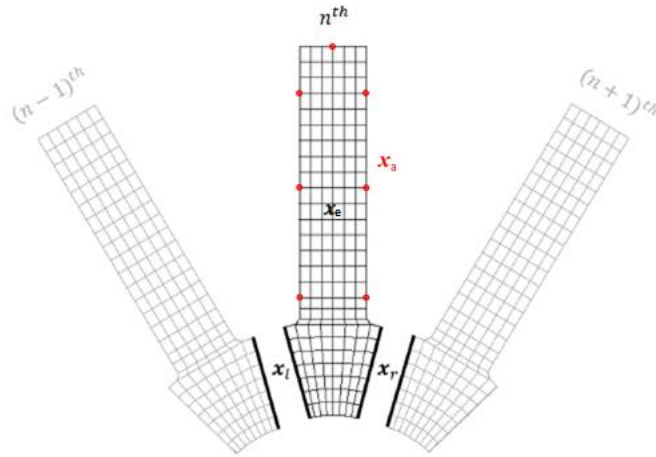


Figure 5.1: Sector of Blade with node for reduction

Usually the coupling of the substructures takes place through the interface displacement. In the case of very complex structures, the size of the system is important and therefore the displacements of the structure must be included in the degrees of freedom "master". The Tran method is suitable for dynamic analysis of turbine sectors as it combines the reduction techniques described above. The result of this method is a condensation of the model and therefore a decrease in calculation times.

The steps to follow are described below:

1. Selection of the "Master" nodes, taking the accessory and left and right interface nodes on the n^{th} sector.
2. Craig-Bampton reduction of the considered sector, taking as "master" nodes those previously selected.
3. Guyan reduction of the considered sector, taking as master nodes only those of right and left interface.
4. Application of cyclic symmetry on reduced models, which consists in expressing the nodes of the right interface according to those on the left.

For the Craig-Bampton model:

$$\{x_{CB}\} = \begin{Bmatrix} x_a \\ x_l \\ x_r \\ \eta_k \end{Bmatrix} = \begin{bmatrix} I & 0 & 0 \\ 0 & I & 0 \\ 0 & Ie^{i\varphi_h} & 0 \\ 0 & 0 & I \end{bmatrix} \begin{Bmatrix} x_a^h \\ x_l^h \\ \eta_k^h \end{Bmatrix} = R_{CB,cs}^h \cdot x_{CB,cs}^h$$

For the Guyan Model:

$$\{X_G\} = \begin{Bmatrix} x_l \end{Bmatrix} = \begin{bmatrix} I \\ Ie^{i\varphi_h} \end{bmatrix} x_l^h = R_{G,cs}^h \cdot x_{G,cs}^h$$

the only unknown factor to be found is x_l .

5. Calculation of x_l by solving the reduced model equation of Guyan using an eigenvalue problem:

$$M_{G,cs} \ddot{x}_l^h + K_{G,cs} x_l^h = f_{G,cs}$$

$$(K_{G,cs} - \omega_j^2 M_{G,cs}) \phi_j = 0 \quad j = 1, \dots, n_l$$

To further reduce the model, a further approximation is made. Approximates the response of the n_l degrees of freedom with the first n_u interface modes or modes of Tran

6. Combination of the two models

$$x_{CB,cs}^h = \begin{Bmatrix} x_a^h \\ x_l^h \\ \eta_k^h \end{Bmatrix} = \begin{bmatrix} I & 0 & 0 \\ 0 & \Phi_u^h & 0 \\ 0 & 0 & I \end{bmatrix} \begin{Bmatrix} x_a^h \\ \eta_u^h \\ \eta_k^h \end{Bmatrix} = T \cdot x_T^h$$

5.5 Contact Analysis

The parameters to be monitored to perform an analysis are those that go to consider some properties related to the material and the type of processing performed. Other parameters, on the other hand, also take into account the amount of energy dissipated by friction.

These parameters are described below:

- Damping Ratio

$$\zeta = \frac{\omega}{\omega_0}$$

This coefficient takes into account the non-linearity due to the microscopic characteristics of the material, such as micro-frictions. These non-linearities are present inside the structure, and therefore are always slightly damped.

ω is the natural frequency of the damped system and ω_0 is the natural frequency of the non-damped system.

Theoretically this parameter must be calculated experimentally, but in our case, we will use a standard constant value valid in general for turbine steels.

- Coefficient of Friction

This is a fundamental parameter as it takes into consideration the amount of rubbing between the contact surfaces. The higher the friction, the lower the sliding and therefore the forced response is more linear. The coefficient of friction depends on the type of material, the temperature and the loads involved.

- Contact Stiffness

In the tool used, this parameter serves to mathematically represent the phenomenon whereby the body deforms due to the contact force before it crawls.

Therefore there is a contact force which is opposed to the motion equal to

$$\begin{Bmatrix} F_u \\ f_v \end{Bmatrix} = \begin{bmatrix} K_u & 0 \\ 0 & K_v \end{bmatrix} \begin{Bmatrix} u \\ v \end{Bmatrix}$$

Where u and v are the relative displacements.

The higher the stiffnesses, the more rigid the system will be and therefore the higher the resonance frequencies will be.

5.5.1 Shroud Contact

the type of blade used for the analysis is the one with contact to the shroud. We can enclose the type of contact in 3 different groups in the type of constraint imposed on the contact:

1. Free: this is the case in which the blade is bound only to the dovetail and therefore there is no contact at the tip. This configuration is the least rigid and therefore the blade moves freely, producing lower frequencies.

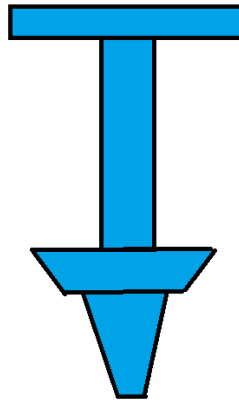


Figure 5.2: Free Contact

2. Tight: in this case the contact surfaces are perfectly welded and therefore there can be no damping. This is the most rigid case and therefore the frequencies will be the highest possible.

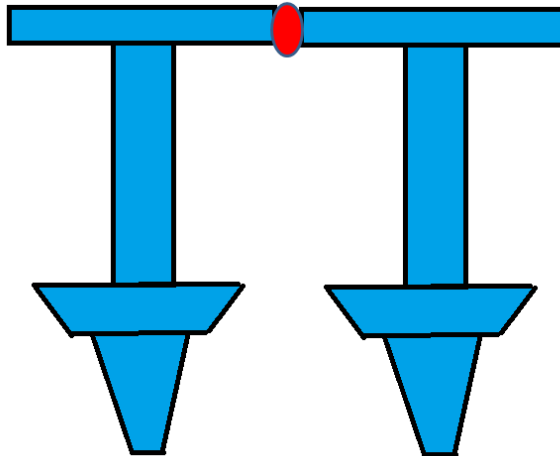


Figure 5.3: Tight Contact

3. Full-Stick: this is the intermediate case between the two. In this condition a certain local deformation is admitted at the contact surfaces.

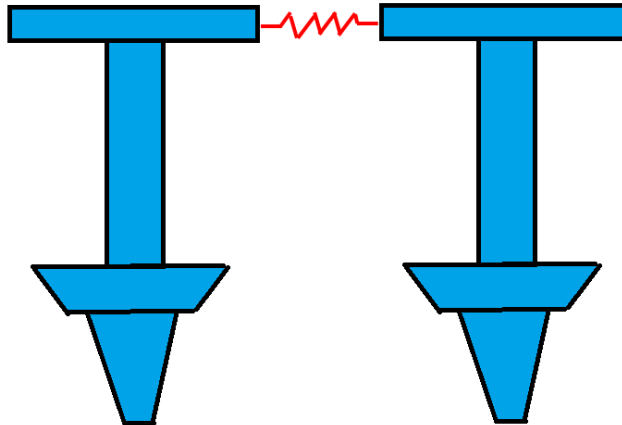


Figure 5.4: Full-Stick Contact

In the event of contact, the points where I simulate the contact must be provided. The surface involved in the contact influences the frequency response. An important variation of the frequencies, instead, is given by the value of the contact stiffness. This influence is noticeable only in the Full-Stick case. Some examples are shown below

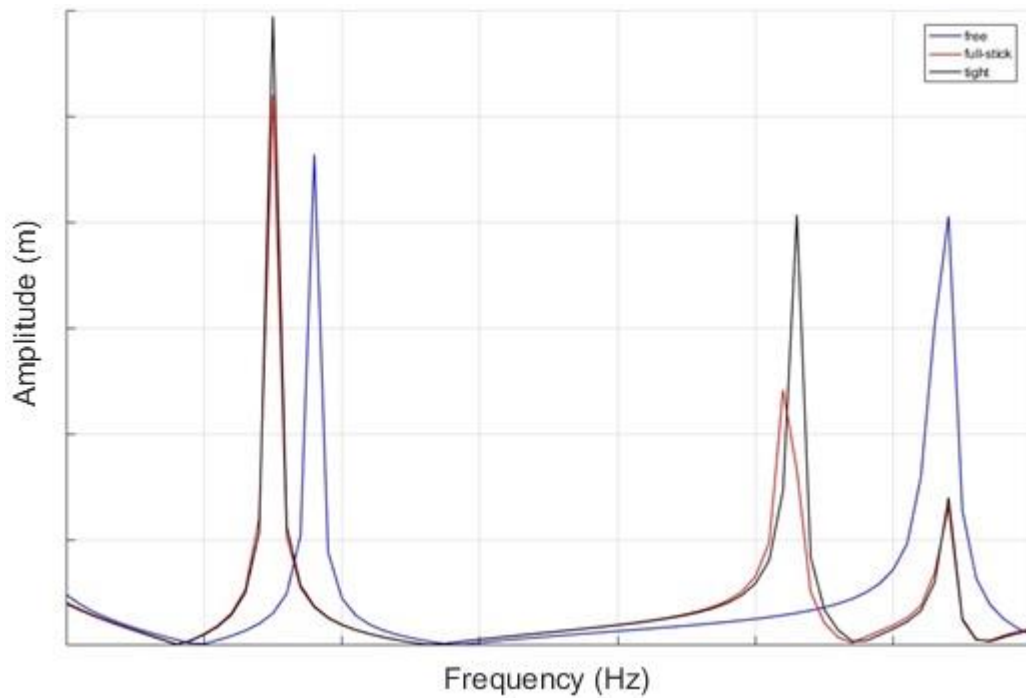


Figure 5.5: Frequency response with stiffness $K=K_{nominal}$

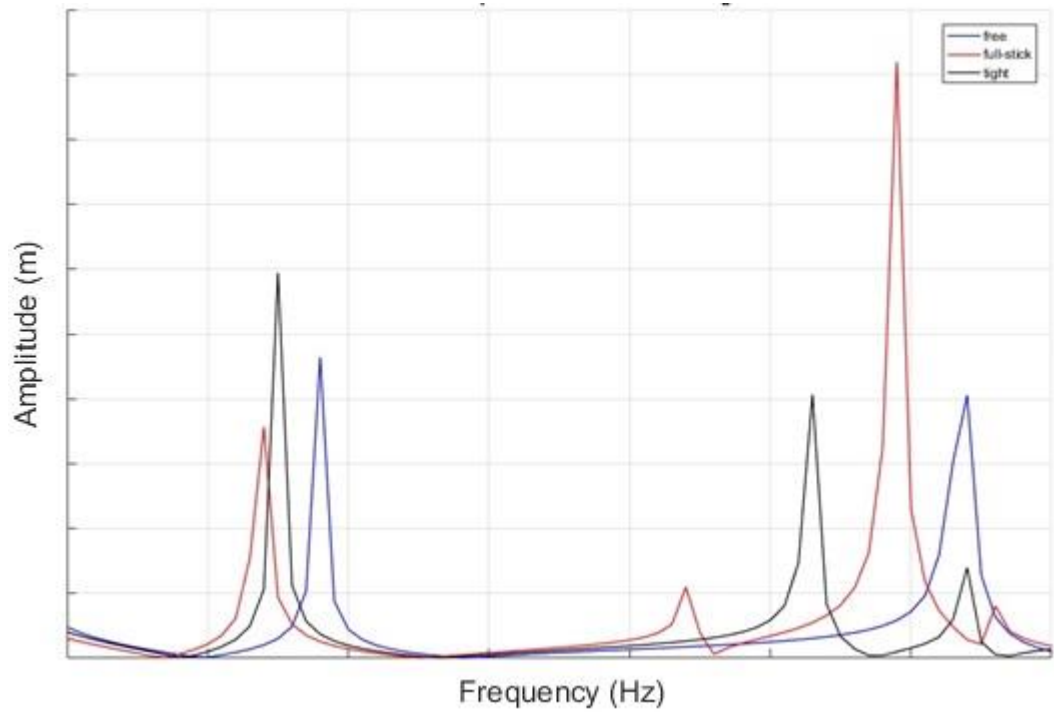


Figure 5.6: Frequency Response with Stiffness $K=0.1 K_{\text{nominal}}$

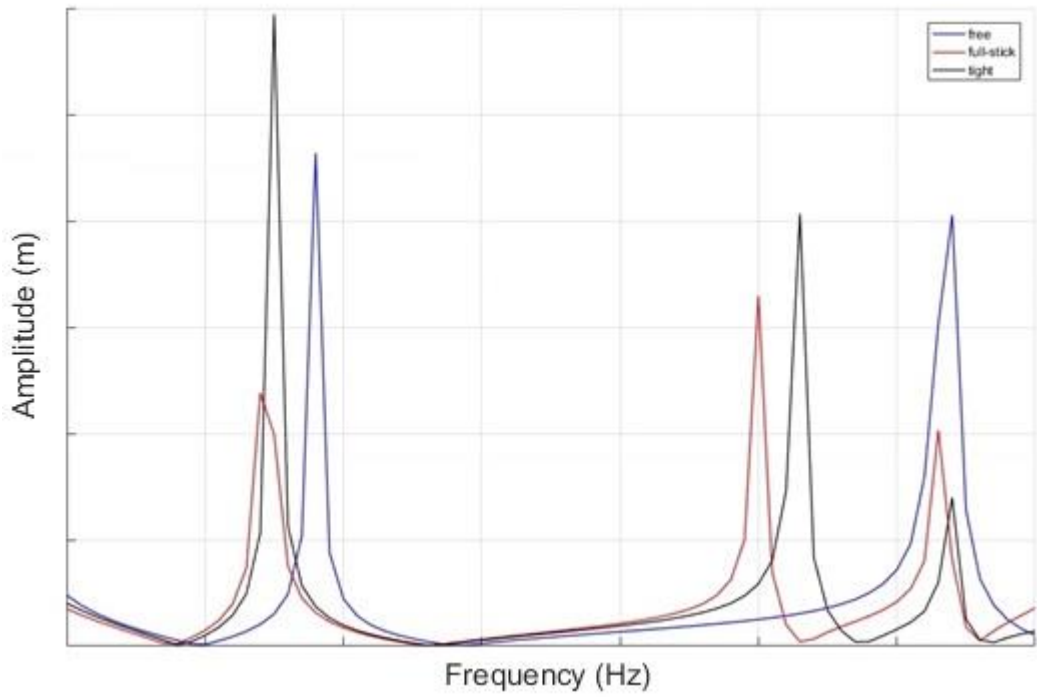


Figure 5.7: Frequency Response with Stiffness $K=0.25 K_{\text{nominal}}$

As can be seen from the graphs, as the contact stiffness increases, the Full-Stick condition gets closer and closer to the Tight condition. However it is not possible to infinitely increase this stiffness because it would lead to non-convergence in the non-linear analysis of the frequency response. On the contrary, by decreasing the stiffness, the frequencies are lowered because the contact deforms more before crawling and therefore is less rigid.

5.5.2 Fem vs Rom

As mentioned above, reduction techniques are advantageous in computational costs, but they introduce a certain error on the results. This error must be evaluated in order to check the quality of the reduction. For this reason, before conducting non-linear analyzes, it is necessary to compare the frequencies obtained with the non-reduced FEM model, and those obtained with the reduced model.

5.5.3 Frequency comparison

The Free and Tight frequencies obtained are compared with those of resonance obtained by Nastran. For a reduction to be considered optimal, the error between these frequencies must be below 1%. Another check to make is to check that the reduced model frequencies, being more rigid, are higher than the unreduced model.

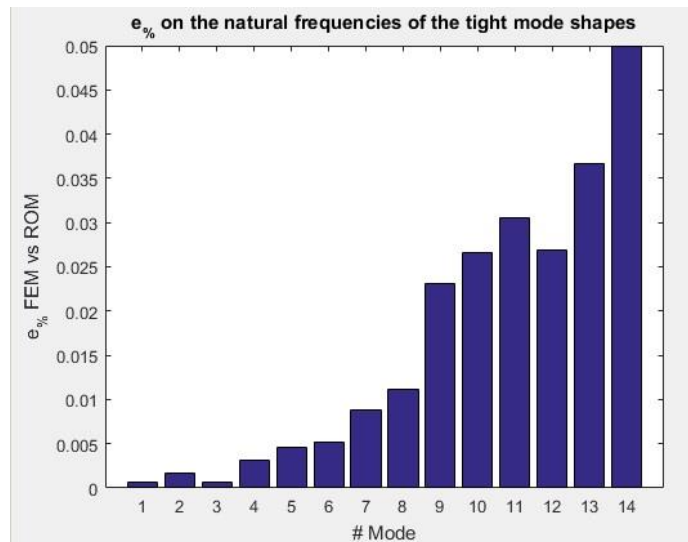


Figure 5.8: FEM vs ROM frequency

5.5.4 Eigenvectors Comparison

There is also a check on the eigenvectors for two groups of "master" nodes, taking the accessory nodes and the right and left interface nodes. The method used is called MAC (Modal Assurance Criterion) which compares the ways of deforming the blades. More the modes will be similar, more the MAC will tends to unity.

$$MAC = \frac{\|\phi_{CB}^T \cdot \phi_{GS}\|^2}{(\phi_{CB}^T \cdot \phi_{GS})(\phi_{CB}^T \cdot \phi_{GS})}$$

Where ϕ_{CB} and ϕ_{GS} are the physical partitions of the eigenvectors of the Craig-Bampton model and the FEM model.

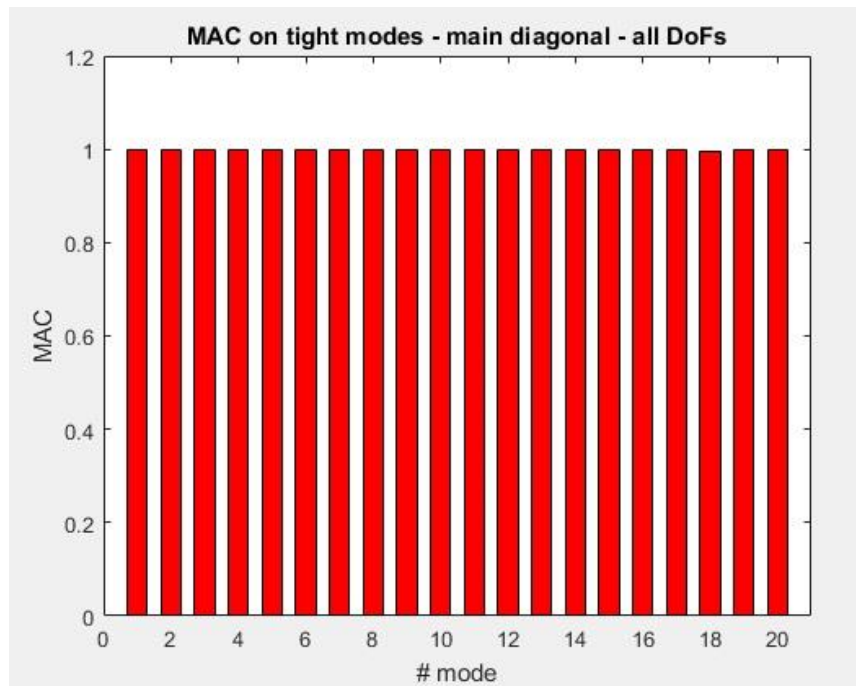


Figure 5.9: FEM vs ROM Eigenvectors

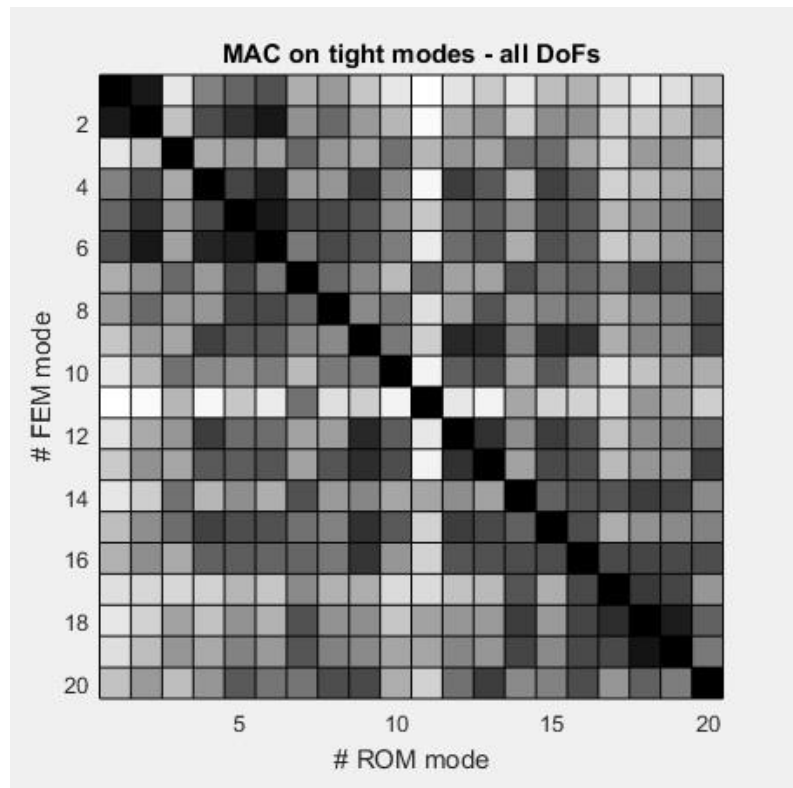


Figure 5.10: MAC diagram

5.5.5 Contact Model

In order to carry out a correct non-linear analysis, the problem of contact must be taken into consideration. The contact must be modeled as correctly as possible. The contact must correctly simulate the actual behavior of the dampers. In the case in question, contacts with a constant normal load varying over time are studied.

Constant normal load

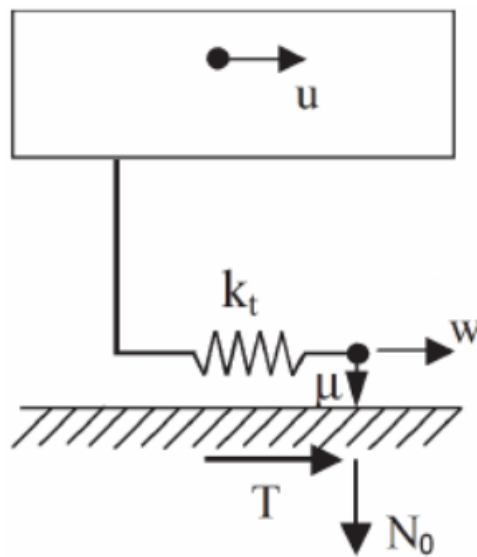


Figure 5.11: Contact Model

A 1D contact model was considered which can simulate the relative tangential displacement under the effect of the constant normal load. With u the relative displacement between the contact nodes is indicated, while with w the displacement of the slider. The stiffness of contact is instead represented by a stiffness spring k_t . N_0 is the normal load.

If the displacement u is different from zero, then the contact begins to deform without slipping. The force T follows the following formula:

$$T = k_t(u - w)$$

The moment the tangential force reaches the "Coulomb limit" the contact begins to creep while maintaining the deformation state in which it is located.

$$F_c = \mu \cdot N_0$$

At the moment in which the displacement u is such as to cancel the slip speed \dot{w} , the contact stops slipping and returns to the stick conditions. By reversing the speed direction \dot{u} , the model gradually returns to the undeformed condition.

It is also possible to evaluate the influence of some parameters that come into play.

By increasing the contact stiffness, the displacement required to reach the Coulomb limit is reduced and therefore the contact first enters the slip.

Instead increasing the friction coefficient, the Coulomb limit also increases and therefore it is necessary to have a greater displacement for there to be creeping. The same thing happens if you increase the normal load.

6. Data Reception Procedure

The best way to know the dynamic response of the various rotor components of a turbine is to perform an experimental test. However, this operation involves a great use of resources, time and costs. To be able to verify correctly, however, the reliability of the analysis performed, it is necessary to make a comparison between the analytical model obtained and the experimental model. In order to make an analytical-experimental comparison, it is necessary to establish the various methods of receiving and processing data.

6.1 Strain Gauges

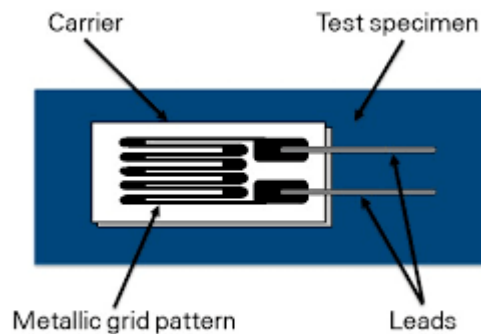


Figure 6.1: Strain Gauge

The extensometer is a measuring instrument used to detect small deformations of a body subjected to mechanical or thermal stresses. Knowing the physical and mechanical characteristics of the material, by measuring the deformation it is possible to obtain the loads to which the material is subjected. Strain gauges are sensitive to the main measurement direction, in fact there are various types to measure various stress conditions. The electric resistance extensometer is the most used since it has excellent general characteristics. It consists of a very thin wire grid rigidly applied to a plastic support. This extensometer is glued on the surface of the body whose deformations are to be measured. The extensometer wire follows the

deformations of the surface to which it is glued, elongating or shortening together with it.

So in function of the deformed that you want to go to study, the extensometer will be positioned on the component with a certain orientation. In general, several strain gauges positioned differently are placed on the same blade.

6.2 Experimental Campbell

In the experimental test, the strain gauges return the trend of deformations or tensions in the time domain. Then we move on to the frequency domain thanks to the use of Fourier series developments. The result of the process is the experimental Campbell diagram. From the graph we note the resonance peaks, for each of which we derive amplitude and Q-Factor.

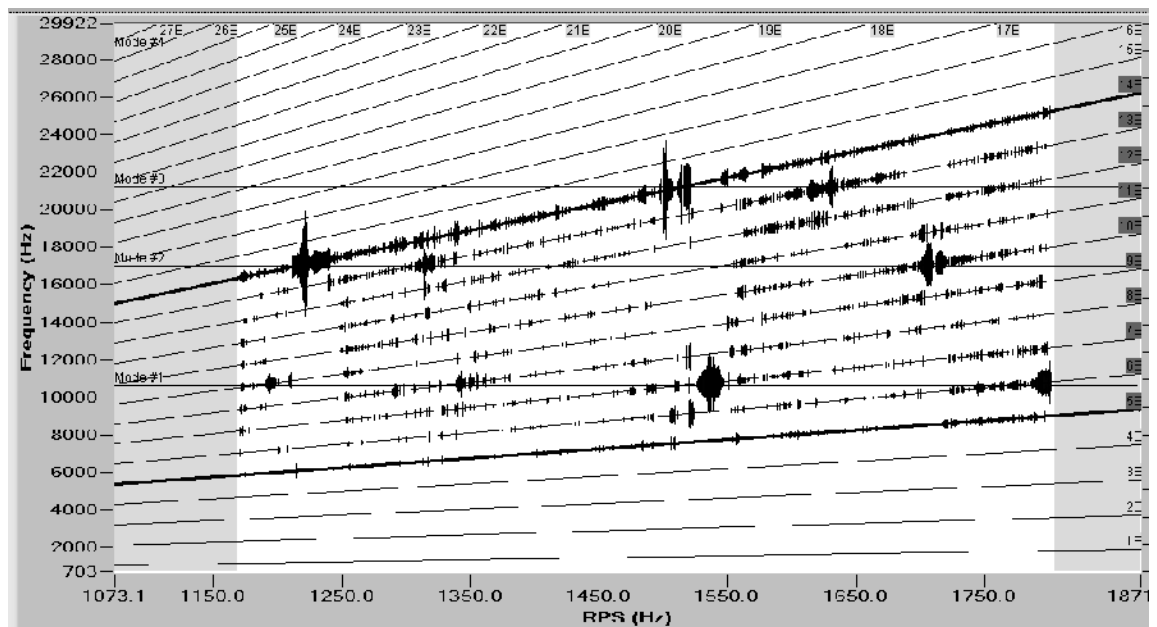


Figure 6.2: Experimental Campbell Diagram

Once the experimental Campbell diagram has been obtained, verification is possible. However, the width read by the diagram is not comparable with the peak obtained from the program as:

1. The experimental data are deformations or tensions, while we need the displacements.
2. The position of the extensometer does not always coincide with the accessory node in which the frequency response is calculated.
3. The strain gauge detects local deformations

So to carry out a comparison, it is necessary to perform a scaling on the experimental results. To do this, a system of local axes is created on the starting model for each Strain Gauge considered. This reference system must follow the curves of the airfoil as much as possible and one of the three axes of the reference system must be directed in the same reading direction as the Strain Gauge.

By considering:

$$u_{FEM} = \text{displacement read by FEM}$$

$$\sigma_{fem} \text{ or } \epsilon_{fem} = \text{Stress or Strain read by FEM}$$

$$\sigma_{EXP} \text{ or } \epsilon_{EXP} = \text{experimental Stress or Strain}$$

Given these values it is possible to calculate the scaling factor.

$$S = \frac{\sigma_{EXP}}{\sigma_{FEM}} = \frac{\epsilon_{EXP}}{\epsilon_{FEM}}$$

this value derives from the relationship

$$\frac{u_{FEM}}{u_{EXP}} = \frac{\sigma_{FEM}}{\sigma_{EXP}} = \frac{\epsilon_{FEM}}{\epsilon_{EXP}}$$

Obtaining: $u_{EXP} = S \cdot u_{FEM}$

In this way it is possible to make a comparison between experimental data and analytical data.

The Q-Factor, on the other hand, is a measure of the degree of damping achieved by the system.

$$Q = \frac{\omega_0}{\Delta\omega}$$

Where $\Delta\omega$ is the value of the distance between two points of the curve whose amplitude value is equal to $A_{MAX}/\sqrt{2}$

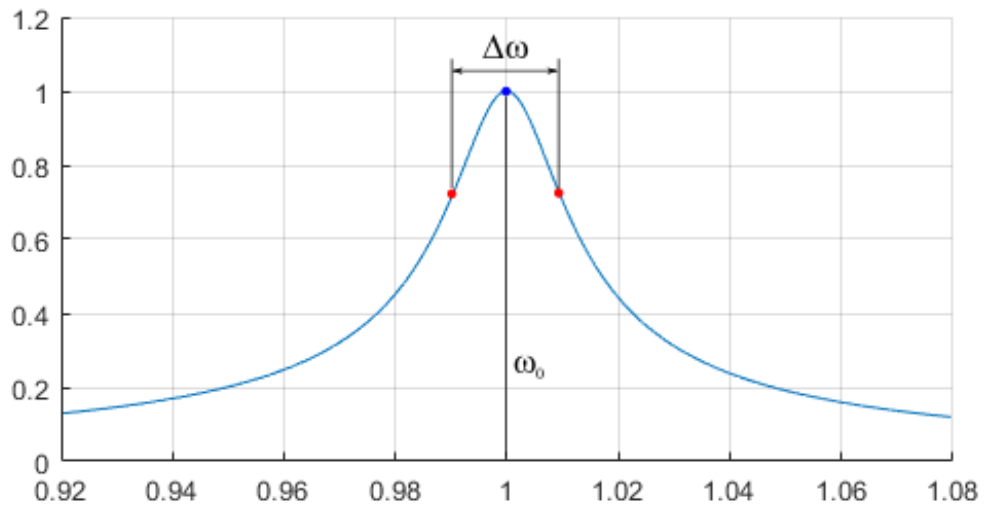


Figure 6.3: Q-Factor Diagram

6.3 TEST CASE

The test case analyzed is an intermediate stage of a low pressure turbine. The type of blade analyzed is connected to the disc via the dovetail. To model the blade a meshing of the various components was performed, guaranteeing a minimum number of nodes and elements, so that the simulation can be considered valid. The contact with the adjacent blades occurs through a simple contact to the Shroud.



Figure 6.4: CAD of sector blade

Before the non-linear analysis, two modal analyzes were performed both in free and in tight condition. Recall that the free condition is that in which the blade is not bound to the tip and is therefore free to vibrate. The tight condition constrains the contact on the whole surface instead. The results of these analyzes correspond to the

boundary conditions on the basis of which the non-linear forced response is then calculated.

Subsequently the model is reduced and the analysis shown in the previous chapters is made, paying particular attention to the master nodes.

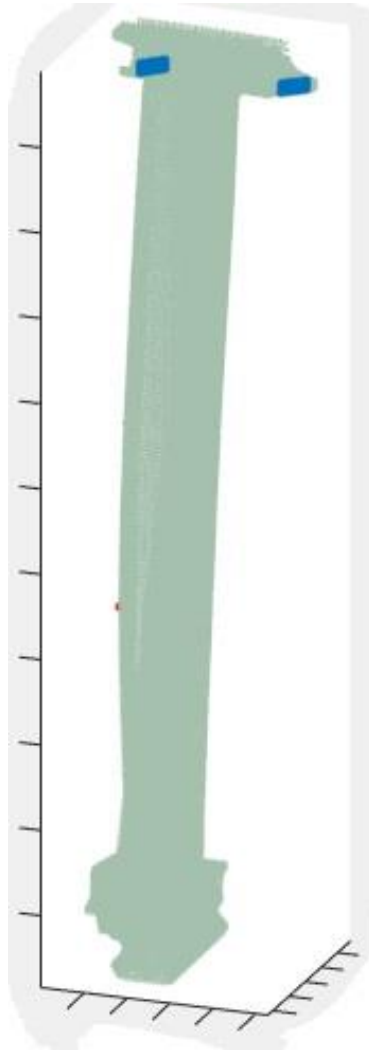


Figure 6.5: Master Node on Blade

The non-linear analysis of the reduced model is carried out taking into account the range of frequencies of interest. The range of frequencies is imposed by the experimental Campbell obtained previously. A first check to perform is to evaluate the experimental frequencies with the frequencies obtained from the FEM model.

The analyzed vibration mode is represented by the following figure.

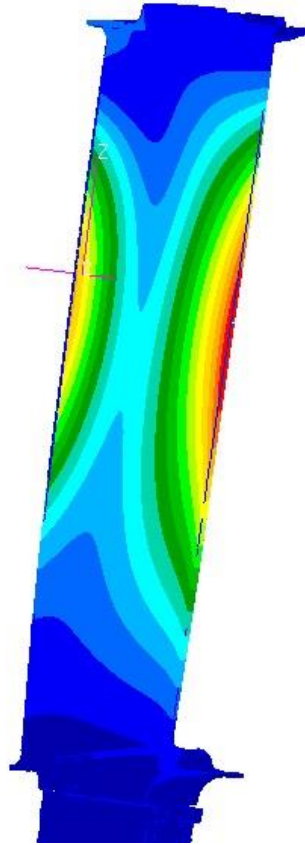


Figure 6.6: Mode Shape

Not having a CFD forcing available, a constant forcing is used in a very precise point of the airfoil.

Being an iterative work, the analyzes are carried out keeping certain parameters fixed and varying others. The goal is to find an optimal solution of parameters that reflects reality as much as possible. The first way to proceed is to set a friction coefficient suitable for the type of material making up the blade, and to vary the contact stiffness and contact force.

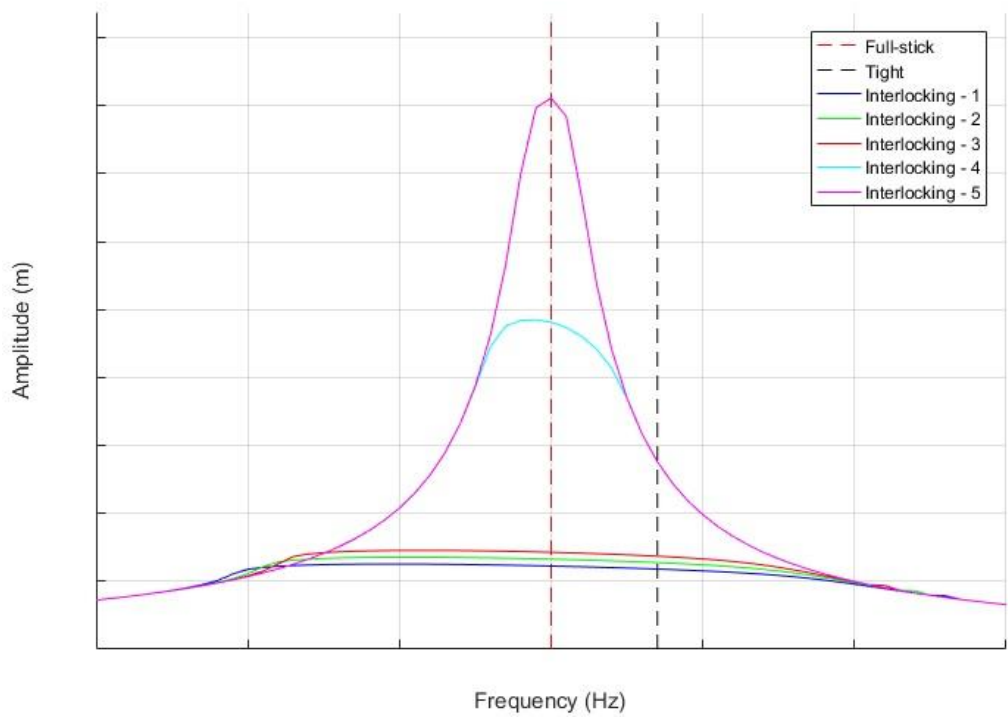


Figure 6.7: Amplitude Diagram

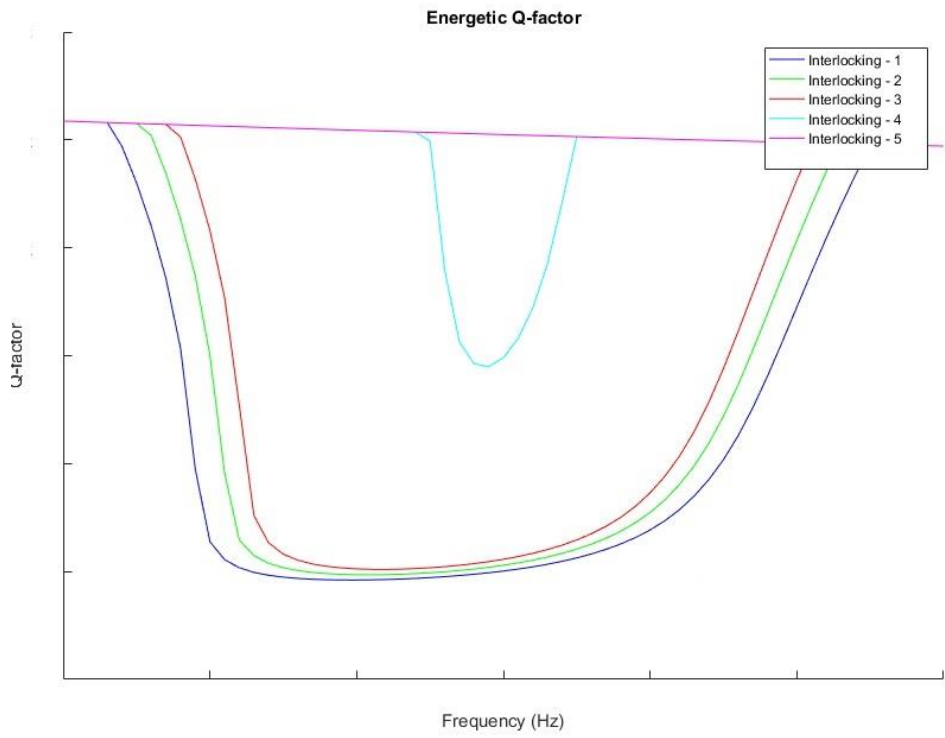


Figure 6.8: Q-Factor Diagram

As can be seen, by increasing the value of contact force, the curves tend to rise. We also see the same behavior in the Q-Factor curve. This behavior can be explained in the following way: by increasing the contact force, we impose on the surfaces a smaller possibility of crawling and therefore a lower ability to dampen the forcing.

Once the first preliminary analysis has been made, the comparison is made with the experimental data. This experimental datum is identified by the Strain Gauge which gave a more acceptable reading for the modal form of interest. The value obtained is then multiplied by the Scale Factor thus making it comparable with the diagrams obtained previously.

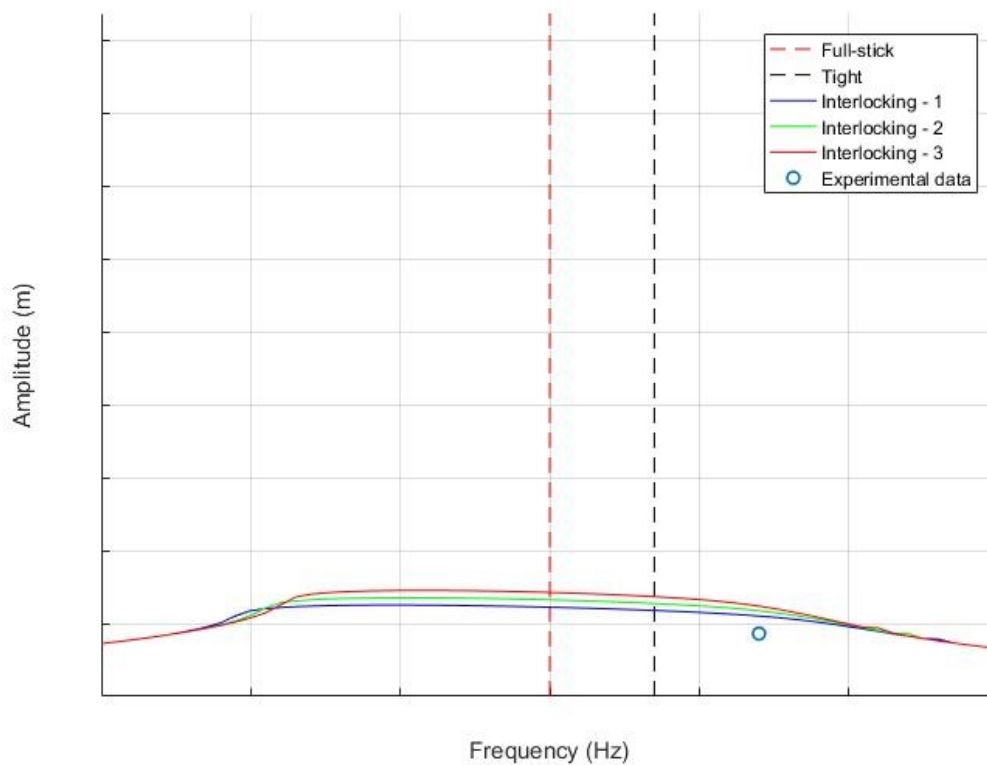


Figure 6.9: Amplitude with Experimental Data

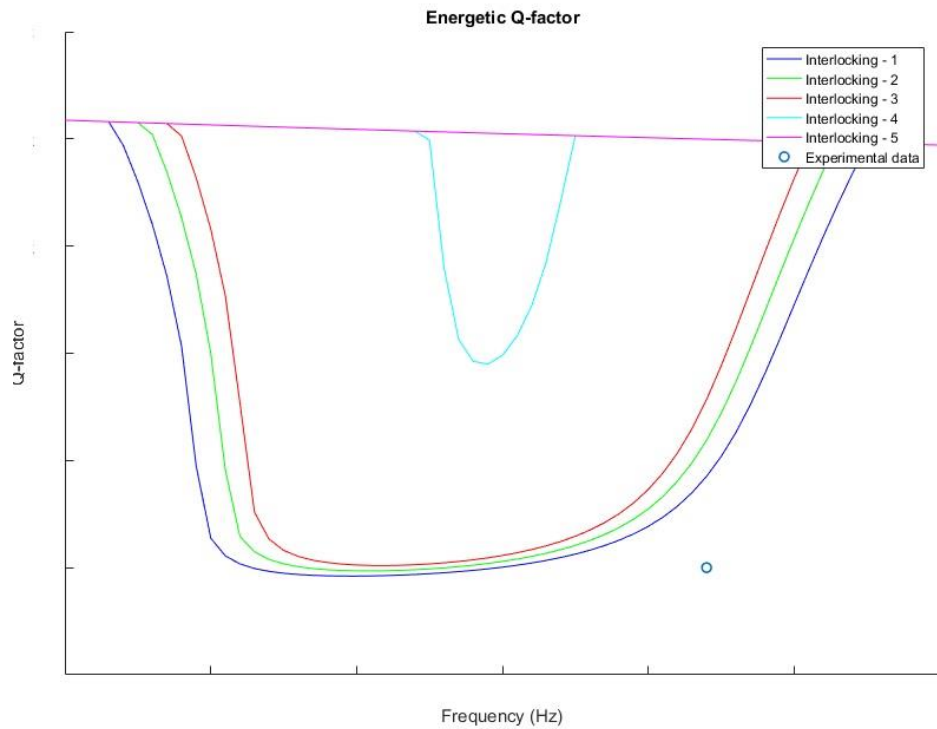


Figure 6.10: Q-Factor with experimental data

From the graphs it would seem that the response of the system is overestimated. The difference instead is less marked in the Q-factor. The frequency obtained instead is very close to that found by the experimental data.

However, considerations can be made in this regard. The first thing is that the analysis was carried out in cyclic symmetry and, as mentioned above, this hypothesis is not applicable to reality as there is no shovel identical to another both at the material level and at the manufacturing level. The second thing is that the calculation of the forcing was carried out considering a point load, and not actually considering the CFD load that the blade suffers.

7. Conclusion

During the thesis process, numerous analyzes were carried out both on FEM models and on reduced models. Initially the main difficulty was in learning the use of software and concepts behind the study of a low pressure turbine stage. Once the path to be followed has been identified, numerous analyzes have been carried out, identifying the main parameters that influence the response of a system.

The main problem was found in identifying the boundary conditions. The results vary greatly as the boundary conditions change. Particular attention has been paid to the correct use of thermal loads and inertial loads.

A further criticality was found in the screening of the contact area at the interlocking. Varying the point where two adjacent blades contacted changes the frequency and the forced response very much.

Finally, the precision in the solution also depends on the type of Strain gauge that is taken into consideration since, analyzing the data of a strain gauge that measures one type of modal form rather than another, it results in an error in the analysis.

Bibliography

- [1] Avio Aero : www.avioaero.com
- [2] General Electric Aviation: www.geaviation.com
- [3] Great 2020: www.great2020.it
- [4] Lorenzo Casalino e Dario Pastrone. <<Fondamenti di macchine a propulsione>>
- [5] Wikipedia
- [6] MSC Software (Patran, Nastran): web.mscsoftware.com
- [7] Altair HyperWorks (Hypermesh): www.altairhyperworks.com
- [8] <<Design of the blisk of an aircraft turbojet engine and verification of its resonance free operation >>L. Chromek
- [9] Appunti Aeroelasticità Prof. Carrera, Politecnico di Torino
- [10] Giuseppe Battiato. <<Vibrations Prediction and Measurement of Multi-Stage Bladed Disks with non Linear Behavior due to Friction Contacts.>> PhD Thesis
- [11] Marsilio. Dispense del corso di Progettazione di motori aeronautici, Politecnico di Torino, 2017-2018
- [12] Amedeo Ramieri. <<Analisi e comparazione di diversi modelli di contatto all'interlocking per rotori di turbine di bassa pressione>>2017
- [13] Giulia Breschi. <<Analisi dinamica e stabilizzazione a Flutter di uno stadio di turbina di bassa pressione>> 2019
- [14] Miriam Zazza. <<Validazione del software Policontact per il calcolo della risposta forzata di componenti aeronautici in presenza di contatti per attrito>> 2019
- [15] Riccardo Scarpulla. <<Metodologia avanzata per la simulazione aeromeccanica di LPT per motori aeronautici commerciali>>2019